Spinal Cord Phosphoproteome of SCA2 Mouse Model Reveals Alteration of ATXN2-N-Term PRM–SH3–Actin Interactome and of Autophagy

Authors

Luis-Enrique Almaguer-Mederos, Arvind Reddy Kandi, Nesli-Ece Sen, Júlia Canet-Pons, Luca-Malena Berger, Matthew P. Stokes, Kathryn Abell, Jana Key, Suzana Gispert, and Georg Auburger

Correspondence

auburger@em.uni-frankfurt.de

In Brief

Polyglutamine-expanded ATXN2 triggers toxic protein interactions and disrupts autophagy in SCA2. Phosphoproteomic profiling of spinal cord tissue from Atxn2-CAG100-KIN mice reveals key phosphorylation changes in ALS-related proteins and autophagy regulators. Findings suggest abnormal polyQ–proline–SH3 interactions as a central disease mechanism, resembling Huntington's pathology.

Graphical Abstract

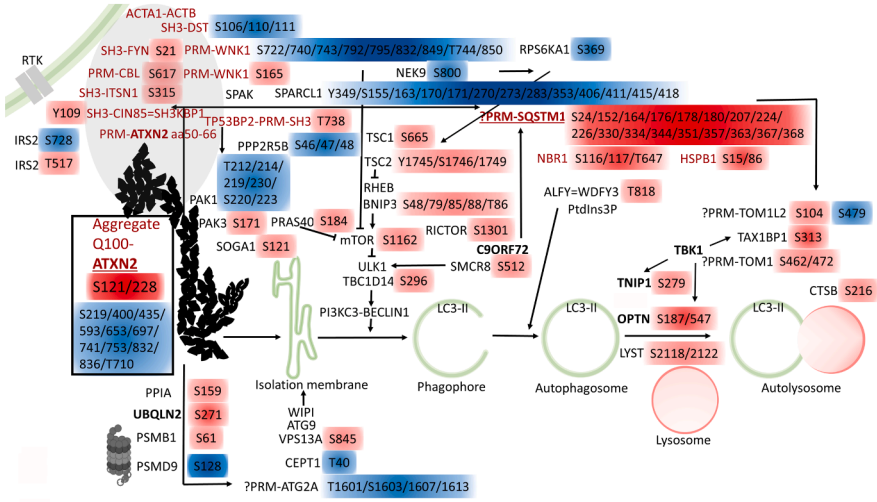

Highlights

- Hyperphosphorylations in polyQ-expanded ATXN2 have pathophysiological implications.
- PolyQ-expanded ATXN2 triggers phosphorylation with enrichment among SH3 proteins.
- Excessive autophagy in SCA2–ALS13 seems to be a primary phenomenon.

2025, Mol Cell Proteomics *24*(*11*), 101072

https://doi.org/10.1016/j.mcpro.2025.101072

Spinal Cord Phosphoproteome of SCA2 Mouse Model Reveals Alteration of ATXN2-N-Term PRM–SH3–Actin Interactome and of Autophagy

Luis-Enrique Almaguer-Mederos[1,‡], Arvind Reddy Kandi[1,‡], Nesli-Ece Sen[1], Júlia Canet-Pons[1], Luca-Malena Berger[1], Matthew P. Stokes[2], Kathryn Abell[2], Jana Key[1], Suzana Gispert[1], and Georg Auburger[1,*]

Toxic polyglutamine (polyQ) expansions in ataxin-2 (ATXN2) trigger neurodegenerative processes, causing spinocerebellar ataxia type 2, and enhancing TAR DNA-binding protein 43–dependent pathology in amyotrophic lateral sclerosis/frontotemporal dementia. Primary disease events can be compensated transiently, delaying disease manifestation. To define potential therapy targets, here we studied how cells modify phosphoprotein signals, using preferentially affected nervous tissue from end-stage *Atxn2*-CAG100-Knockin mice. The spinal cord phosphoproteome revealed massive hyperphosphorylations flanking the polyQ expansion in ATXN2 and for SQSTM1 and moderate hyperphosphorylations also for amyotrophic lateral sclerosis proteins, OPTN (optineurin), UBQLN2 (ubiquilin-2), TNIP1 (TNFAIP3 interacting protein 1), and TBK1-targeted TAX1BP1. Conversely, strong hypophosphorylations of WNK1 (protein kinase with no lysine 1), SPARCL1 (secreted protein acidic and cysteine rich-like 1), and PSMD9 (proteasome 19S regulator non-ATPase assembly chaperone P27) were found. Significant enrichments of SRC-homology domain type 3–containing proteins, autophagy/endocytosis factors, and actin modulators could be explained by N-terminal, polyQ-adjacent, proline-rich motifs in ATXN2, suggesting that spinocerebellar ataxia type 2 pathogenesis is highly similar to Huntington's disease, where neurotoxicity is mediated by abnormal polyQ–proline-rich motif–SRC-homology domain type 3 interactions. Validation of protein and mRNA levels was done in mouse spinal cord and embryonic fibroblasts or patient fibroblasts after bafilomycin or arsenite treatment, observing polyQ-dependent OPTN deficiency and SQSTM1 induction impairment. Overall, this phosphoproteome profile identified and quantified the main cellular efforts in adapting autophagy pathways to the aggregation propensity of the ATXN2-N-term.

Spinocerebellar ataxia type 2 (SCA2) is a rare neurodegenerative disorder with autosomal dominant inheritance, caused by a cytosine–adenine–guanine (CAG)n repeat expansion mutation in the ataxin-2 (ATXN2) gene (human gene symbol *ATXN2*, chromosomal cytogenetic band 12q24.12), encoding an expanded polyglutamine (polyQ) tract near the N-terminus of ATXN2 protein (1–3). Repeat expansions beyond (CAG)32 repeats lead to typical spinocerebellar manifestation by affecting glutamatergic synapses preferentially. This occurs in two main areas: in the spinal cord, where it impacts connections between upper and lower motor neurons, and in the cerebellum, where it disrupts the synapses between granule neuron parallel fibers and the dendritic trees of Purkinje neurons. Subsequent atrophy of further neuronal circuits, denervation of skeletal muscles, and demyelination, with final patient immobility, lead to a characteristic combination of tremor, leg cramps, slowed saccadic eye movements, decreasing body mass index, and death within 30 years after clinical manifestation (4–8). While unable to cause the monogenic, fully penetrant SCA2, the intermediate-length expansions with size (CAG)27-32 act within polygenic networks to increase the disease risk and/or progression of 1) amyotrophic lateral sclerosis (ALS or ALS13) (9–14), 2) frontotemporal dementia (FTD) (15–17), 3) tauopathies named as progressive supranuclear palsy or as Parkinson plus (18), and also 4) idiopathic Levodopa-responsive Parkinson's disease (19). ALS and FTD display a characteristic neuropathological combination of cortical and spinal motor neuron degeneration in the absence of cerebellar

From the [1]Goethe University Frankfurt, University Hospital, Clinic of Neurology, Frankfurt am Main, Germany; and [2]Cell Signaling Technology Inc., Danvers, Massachusetts, USA

‡These authors contributed equally to this work.

*For correspondence: Georg Auburger, auburger@em.uni-frankfurt.de.

https://doi.org/10.1016/j.mcpro.2025.101072

atrophy, with the appearance of cytosolic inclusion bodies that contain the normally nuclear ribonucleoprotein (RNP) TAR DNA-binding protein 43 (TDP-43) as a hyperphosphorylated, ubiquitinated, and proteolytically cleaved C-terminal fragment (20, 21). This RNP–RNA aggregation process in ALS–FTD usually occurs without colocalization of expanded ATXN2, except transiently in individual patients (22–25).

In view of the causal neurotoxic role of ATXN2 for SCA2, and of its modifier role for ALS and FTD, the most promising approaches toward their preventive neuroprotective treatment are focused on repressing the expression of *ATXN2* mRNA. Successful preclinical studies showed the KO of murine ATXN2 to extend the survival of TDP-43-overexpressing mice from 20 days to more than 2 years (26). The *in vivo* administration of antisense oligonucleotides (ASOs) or Cas13 CRISPR effectors to eliminate murine *Atxn2* mRNA was found to improve functional deficits, extend survival, and reduce neuropathology in ALS models (26–28). Similarly, preclinical studies conducted in SCA2 mouse models also showed ASO intrathecal delivery as a promising disease-modifying treatment for this condition (29). Furthermore, the identification of small drugs that minimize ATXN2 expression was beneficial in an SCA2 mouse model by normalizing molecular markers of pathology such as the levels of the selective autophagy receptor (SAR) SQSTM1, also known as p62 (30). Conversely, the lentiviral introduction of expanded ATXN2 into the brain triggers the accumulation of LC3-II and SQSTM1 as aggrephagy mediators (31, 32), whereas pharmacological autophagy enhancement is protective in SCA2 models (33). Thus, clinical trials to prevent SCA2 and ALS *via* ATXN2 knockdown approaches have been initiated and will need to be optimized by the identification of the neurotoxic ATXN2 interactions and by the definition of molecular events that serve as biomarkers for progression *versus* regeneration.

What are the binding partners and physiological roles of ATXN2, what is its connection with TDP-43, and how does ATXN2 acquire neurotoxicity upon polyQ expansion? It is relevant to know that the KO of ATXN2 results only in age-associated obesity, hypercholesterolemia, and hepatosteatosis (34–36), whereas the KO of its more abundantly expressed paralog Ataxin-2-like (ATXN2L) causes mid-embryonic lethality (37). Vertebrates (except birds) have developed two independent ATXN2 gene copies, whereas only one gene copy exists from nematode worms (*ATX-2*) *via* fruit flies (d*Atx2*) to yeast (*PBP1*), and land plants like *Arabidopsis thaliana* again have two copies (CID3 and CID4) (38). A strong sequence conservation across eukaryotes is most evident in several functional domains:

i. As a common element in all ATXN2 family members, the poly(A)-binding protein–associated motif 2 (PAM2) and its interaction with the MLLE domain of poly(A)-binding protein 1 (PABPC1) was first identified in yeast. Using this knowledge, various studies convincingly demonstrated the impact of the ATXN2 family on mRNA poly (A) tail length, translation efficiency, and RNP association (39–53).
ii. All ATXN2 family members have a domain with similarity to the Sm (single-strand poly(C)-binding domain in nuclear protein) motif of nuclear splice factors, although ATXN2 and several other proteins with such an LSm (like Sm) domain localize in the cytosol where no splicing occurs (54–56). It was shown that this LSm domain and the LSm-associated domain (LSm-AD) in ATXN2 mediate direct binding and processing of RNAs and interaction with RNA-processing proteins such as the RNA helicase DDX6 (57–60). Together, the PAM2 motif and the LSm domain explain why the ATXN2 family members relocalize with PABPC1–mRNAs–RNPs (*e.g.*, TIA1, G3BP1)/40S ribosome subunits to condensate in stress granules when cellular damage such as oxidative stress or starvation requires the quality control and possibly degradation of RNAs (61–63). The indirect association of ATXN2 with the ALS disease protein TDP-43 is thought to be mediated by RNAs that are associated with the LSm–LSm-AD domains (9, 28, 64).
iii. The presence of a long polyQ domain within ATXN2 is prominent in primates and insects, but shorter polyQ domains appear in most mammalian ATXN2 orthologs, at differing positions (38).
iv. Proline-rich motifs (PRMs) are frequent in several positions among the ATXN2 family members (38). At least four distinct PRMs exist within human ATXN2, two within the main isoform after the polyQ repeat and two or three before the polyQ repeat within the extended N terminus of an alternative longer isoform, usually having the classical sequence **P**XX**P**XXR or RXX**P**XX**P** that can interact with SRC-homology domain type 3 (SH3) domains. Their SH3-containing interactor proteins control actin filament assembly itself or the interaction of actin fibers with the plasma membrane receptor tyrosine kinase (RTK) endocytosis apparatus. Indeed, mostly the third PRM in ATXN2 was demonstrated to associate with the SH3-containing proteins CIN85 (Cbl-interacting protein of 85 kDa), ITSN1, SRC, and Endophilin A1/A3. *Via* this association, ATXN2 repressed the internalization of the epidermal growth factor receptor in peripheral cells and would be expected to have analogous effects on other RTK family members in the nervous system (65–68), so that ATXN2 orthologs from yeast *via* nematodes to mammals were shown to repress the mechanistic target of rapamycin complex 1 (mTORC1) growth signals and cell size, modulating autophagy *via* ULK1 (48, 69–74).

Overall, the principal phenotypes of d*Atx2* mutation in fruit flies are 1) impaired translation because of altered direct association of ATXN2 with polyribosomes and 2) aberrant sensory bristle morphology because of an indirect and poorly characterized influence of ATXN2 on actin filament formation (42, 75). Until the present study, it had remained unclear to what degree these two functions are critical for the disease and how they are affected by the initial partial loss of function or the subsequent neurotoxic and progressive gain-of-function of polyQ expansion disorders.

To model SCA2 and ALS13 disease processes upon ATXN2 polyQ expansion by a genetic approach in animals, we used targeted recombination to perform the knockin (KIN) of a (CAG)100 repeat at the appropriate position of the *Atxn2* gene within the mouse genome. An additional insertion of LoxP sites was performed at either side of the (CAG)100 repeat, which permits the conditional conversion of the KIN-triggered neurodegeneration into a KO that would halt the neurotoxicity and permit partial regeneration once a transgenic Cre recombinase in such mouse mutants is activated by tamoxifen injection at any disease stage (76). This approach was successful in generating the *Atxn2*-CAG100-KIN mouse mutant, where the physiological promoter governs endogenous ATXN2 expression regulation and where the expansion is unstable over generations, just as in patients. Faithfully mirroring the temporal and spatial pattern of SCA2 pathology, the polyQ expansion in ATXN2 is detectable in the central nervous system and peripheral liver tissue of these mutant mice (77–80), triggering initial obesity by the age of 10 weeks (reflecting an initial partial loss-of-function) that develops into weight loss by 10 months (reflecting the subsequent progressive gain-of-function), with clear deficits of vertical movement coordination by the cerebellum from 4 months, and a reduction of grip strength as a reflection of motor neuron degeneration from 9 months onward (77, 81). In the spinal cord, progressive TDP-43 aggregation is observed, together with cholesterol anomalies (81). In the cerebellum, prominent anomalies of calcium and sphingomyelin lipids are documented, as in SCA2 patients (79, 80). Overall, the breeding of homozygous mouse mutants causes a more severe progression than heterozygotes, similar to the unusually strong affection of homozygous SCA2 patients (77, 82–84). The lifespan of the homozygous KIN mice is limited to 14 months, whereas matched WT mice have a life expectancy well beyond 24 months (77). In contrast to SCA2 mouse models with transgenic overexpression of recombinant ATXN2, this KIN mouse can be expected to reflect the anomalies of ATXN2 splicing, proteolytic cleavage, post-translational modifications, and interactor binding in patterns that would be characteristic for the human SCA2 and ALS13 nervous system. Such investigations in patient tissues are usually impossible because of the unavailability of high-quality autopsy material in such rare disorders.

In the present study, a survey of phosphorylation changes was documented in the spinal cord of such KIN mice at the terminal disease stage. As a technical approach, the phosphorylated peptides from a proteolytically cleaved protein extract were bound by iron–nitrilotriacetic acid on immobilized metal affinity chromatography (IMAC) columns, to be subsequently sequenced and quantified by label-free mass spectrometry (MS). We hoped to elucidate how the tyrosine (Tyr, Y) phosphorylations at the receptor endocytosis machinery are adapted and how the cells adapt their stress signaling *via* serine (Ser, S)/threonine (Thr, T) phosphorylation cascades from the plasma membrane to the nucleus, attempting to counteract the specific atrophy process of SCA2 at crucial molecules and pathways.

EXPERIMENTAL PROCEDURES

Experimental Design and Statistical Rationale

In this study, we compared the nervous tissue of four WT mice and sex-/age-matched four *Atxn2*-CAG100-KIN mice employing two technical replicates per sample in phosphoproteomic analyses, six WT *versus* sex-/age-matched six KIN spinal cord samples or five WT *versus* sex-/age-matched four KIN mouse embryonic fibroblast (MEF) lines in RT–quantitative PCR (qPCR), two WT *versus* sex-/age-matched two KIN spinal cord tissues in immunohistochemical staining, and quantitative immunoblots in five WT *versus* sex-/age-matched five KIN spinal cord samples, or four WT *versus* sex-/age-matched four KIN MEF lines, or three controls *versus* sex-/age-matched three SCA2 patient skin fibroblast lines. For the statistical evaluation of the phosphoproteome, ratios for each comparison were generated, converted to $\log_2$ scale, and normalized. *P* Values were calculated using a two-tailed *t* test, and $p < 0.05$ was deemed to achieve nominal significance. The *t* test significance without stringent multiple-testing correction in proteomic profiling can only be considered exploratory, but the effect of reproduction in follow-up experiments with independent techniques and additional biological samples, testing interspecies and intertissue consistency, ensured the validity of the main findings.

Statistical comparisons between the two groups for RT–qPCR and immunoblots were assessed after the application of unpaired Student's *t* tests with Welch's corrections. For bafilomycin treatment of MEF, three biological replicates per group were used, and the statistical analysis was done with two-way ANOVA.

Experimental Animals

All mouse experiments were in conformity with the German Animal Welfare Act, the Council Directive of November 24, 1986 (86/609/EWG) with Annex II and the ETS123 (European Convention for the Protection of Vertebrate Animals). All mice were housed at the Central Animal Facility (ZFE) of Goethe University Medical School, kept in individually ventilated cages with nesting material at a 12 h light–12 h dark cycle, with appropriate temperature and humidity conditions, and provided with food and water *ad libitum*. Breeding of heterozygous carriers was used for colony expansion and maintenance. Among offspring littermates, the homozygous *Atxn2*-CAG100-KIN and WT animals of the same sex were selected and aged together in the same cages for subsequent experimental group comparisons regarding phosphoproteome, gene expression, protein abundance, and immunohistochemistry. Both female and male mice were used

during all experiments. The study was ethically approved by the Regierungspräsidium Darmstadt on March 27, 2017 (number V54-19c20/15-FK/1083).

Genotyping of Atxn2*-CAG100-KIN Mice*

The mouse strains were maintained in the C57BL/6 background. The genotyping of *Atxn2*-CAG100-KIN mice was done as previously described (77). Briefly, genomic DNA was isolated from ear punches or tail biopsies using a standard protocol (85). The CAG repeat was assessed by standard PCR amplification with the NOW1-K2 and NOW1-H2 oligonucleotide primers, TaKaRa LA Taq-Polymerase (Takara Bio, Inc), and a PCR Master Mix containing 2 mM cresol, 250 μM dNTPs, and 60% sucrose in PE buffer. Amplification was performed in a SimpliAmp PCR thermocycler (Applied Biosystems) as follows: initial denaturation at 94 °C for 3 min, followed by 30 cycles of denaturation at 94 °C for 15 min, annealing at 68 °C for 4 min, elongation at 68 °C for 4 min, and a final elongation step at 68 °C for 9 min. PCR products were run in 2% agarose gel electrophoresis, and the TrackIt 100 bp DNA Ladder (Invitrogen) was used to estimate the size of the amplicons. The WT allele produced an amplification product of 793 bp and the expanded CAG100 allele produced a 948 bp amplicon.

Experimental Design of Cell Lines and Their Treatments

MEFs were obtained from WT and homozygous *Atxn2*-CAG100-KIN embryos around E15–18 as previously described (48). For analyses, four different WT and four different KIN lines were used, reflecting biological replicates each, since they stem from individual mouse embryos. Human skin fibroblasts were acquired by biopsing the forearm of three clinically and molecularly diagnosed SCA2 patients and three age- and gender-matched control individuals (67). MEF and human skin fibroblasts were cultured in Dulbecco's modified Eagle's medium (1×) with high glucose (4.5 g/l D-glucose) and sodium pyruvate (0.11 g/l) (Thermo Fisher Scientific; catalog no.: 21969), supplemented with 1% glutamine (Gibco; catalog no.: 25030081), 10% fetal bovine serum (Gibco; catalog no.: A3160802), and 1% penicillin–streptomycin (Gibco; catalog no.: 15140-122) at 37 °C, 5% CO_2, and 95% relative humidity. The fibroblasts were plated in 100 mm dishes and allowed to grow for at least 2 days until they reached 70% to 90% confluency, before being treated with bafilomycin A1 (BafA1) (Sigma; catalog no.: 19-148), sodium arsenite (NaARS) (Sigma; catalog no.: S7400), or their appropriate vehicles (0.5% dimethyl sulfoxide or H_2O, respectively). Fibroblasts were treated overnight (24 h) with BafA1 (20, 60, or 100 nM), dissolved in dimethyl sulfoxide, or NaARS (5 or 10 μM) dissolved in media. An equal number of dishes were treated with the appropriate vehicle only. Cell pellets were obtained by trypsinization and centrifugation.

Experimental Design of IMAC Phosphoproteomics

Mouse cervicothoracic spinal cord tissue was obtained after cervical dislocation, then immediately frozen and transported in liquid nitrogen. Phosphoproteome profiling of spinal cord tissue from four WT *versus* four KIN mice was performed at Cell Signaling Technology, Inc, using their PTMScan and Fe-IMAC services. Samples were first prepared in urea lysis buffer (9 M urea, 20 mM Hepes [pH 8.0] + phosphatase inhibitor cocktail) and then shipped to Cell Signaling Technology for analysis. Four biological replicates of each condition were used for the analysis to account for potential intra-group variability and allow calculation of *p* values for changes observed. Cells were sonicated and centrifuged to remove the insoluble material. Protein content was determined by Bradford assay, and equal protein quantities from all samples were used for analysis. Samples were reduced with DTT and alkylated with iodoacetamide. Input protein (500 μg) from each sample was digested with trypsin (CST; catalog no.: 56296), purified over C18 columns (Waters; catalog no.: WAT051910), and enriched using the PTMScan Fe-IMAC beads (CST; catalog no.: 20432) as previously described (86). Samples were desalted over C18 tips prior to LC–MS/MS analysis.

LC–MS/MS analysis was performed using a Thermo Orbitrap Fusion Lumos Tribrid mass spectrometer as previously described (86, 87) with replicate injections (technical duplicates) of each sample run nonsequentially (injection 1 of samples 1, 2, 3, 4, 5, 6, 7, 8 followed by injection 2 of samples 8, 7, 6, 5, 4, 3, 2, and 1). This allows two opportunities to identify peptides in each sample and provides a measure of analytical reproducibility across the entire sequence of LC–MS/MS runs (shown with % CV values for each peptide across replicate injections). Briefly, peptides were separated using a 50 cm × 100 μM PicoFrit capillary column packed with C18 reversed-phase resin and eluted with a 90-min linear gradient of acetonitrile in 0.125% formic acid delivered at 280 nl/min. Tandem mass spectra were collected in a data-dependent manner using the following parameters: MS1 spectra were collected at a resolving power of 120,000 at *m/z* 200 over *m/z* 300 to 1500 with a standard automatic gain control target and a maximum injection time of 50 ms. The MIPS filter was applied with peptide mode selected. Precursors were filtered to charge states of 2 to 7, and a dynamic exclusion filter was applied with 30 s duration and 10 ppm low and high mass tolerance. MS2 scans were collected in the Orbitrap analyzer at a resolution of 30,000 at *m/z* 200 with a defined first mass of 110 *m/z* and an isolation window of 1.6 *m/z*. A fixed collision energy of 27 was used with a standard automatic gain control and a maximum injection time of 50 ms. Real-time recalibration of mass error was performed using lock mass (88) with a singly charged polysiloxane ion *m/z* = 371.101237.

MS spectra were evaluated by Cell Signaling Technology using Comet and the GFY-Core platform (Harvard University) (89–91). Searches were performed against the 20210303 update of the UniProt *Mus musculus* database containing 25,361 entries with a mass accuracy of ±20 ppm for precursor ions and 0.02 Da for product ions. Partial trypsin cleavage (K/R not KP/RP) was required in the database search. Cysteine carbamidomethylation (C +57.02146374) was specified as a static modification, and oxidation of methionine (M +15.9949146221) and serine, threonine, or tyrosine phosphorylation (S/T/Y +79.966331) were allowed as variable modifications. Up to four missed cleavages and up to four variable modifications were allowed per peptide. Results were filtered to a 1% peptide-level false discovery rate (FDR) with mass accuracy ±5 ppm on precursor ions and the presence of a phosphorylated residue for enriched samples using the linear discriminant module in GFY-Core. Results were further filtered to a 1% protein-level FDR using the Protein Sieve module in GFY-Core. Site localization confidence was determined using Ascore (92). Protein and site data were retrieved from the PhosphoSitePlus database, which uses phosphorylation site numbers from UniProt (93). Links to the protein pages for each identified phosphopeptide are hyperlinked in the "Accession" column of Supplemental Table S1 and are also provided in the URL column for copy/paste into web browsers.

All quantitative results were generated using Skyline (94) to extract the integrated MS1 peak area of the corresponding peptide assignments. Accuracy of quantitative data was ensured by manual review in Skyline or in the ion chromatogram files. A median log2 strategy was used to normalize quantitative data across samples where the intensities in each injection are adjusted based on the median intensity for all peptides in each injection. Minimal normalization was needed, with normalization factors ranging from 1.00 to 1.55 across

all injections. *P* Values were calculated using a two-tailed equal variance (homoscedastic) *t* test in Excel.

RT–qPCR in Spinal Cord and Fibroblasts

Total RNA isolation from spinal cord tissue (6 WT *versus* 6 KIN) and fibroblast pellets (5 WT *versus* 4 KIN lines, reflecting biological replicates) was performed with TRIzol reagent (Sigma–Aldrich) according to the manufacturer's instructions. Total RNA yield and purity were quantified using a Tecan Spark plate reader (Tecan Group Ltd) at 230, 260, and 280 nm in a NanoQuant plate. Complementary DNA synthesis was performed from 1 μg of total RNA template using the SuperScript IV VILO kit (Invitrogen) according to the manufacturer's instructions. Gene expression profiles were assessed by RT–qPCR using a StepOnePlus (96-well) Real-Time PCR System (Applied Biosystems). RT–qPCRs were run in technical duplicates on complementary DNA from 25 ng total RNA, with 1 μl TaqMan Assay, 10 μl FastStart Universal Probe Master 2× (Rox) Mix (Roche), and ddH_2O up to 20 μl of total volume. The PCR cycling conditions were 50 °C for 2 min, 95 °C for 10 min, followed by 40 cycles of 95 °C for 15 min and 60 °C for 1 min. The gene expression TaqMan assays (Thermo Fisher Scientific) used for this study were *Bnip3* (Mm00833810_g1), *Ctsb* (Mm01310506_m1), *Myo6* (Mm00500651_m1), *Nbr1* (Mm01249798_m1), *Optn* (Mm01333245_m1), *Ppia* (Mm02342430_g1), *Sparcl1* (Mm00447784_m1), *Sqstm1* (Mm00448091_m1), *Tax1bp1* (Mm00518038_m1), *Ubqln2* (Mm00834570_s1), *Wdfy3* (Mm00556380_m1), and *Wnk1* (Mm01184014_m1, Mm01184007_m1, and Mm01184011_m1). The data were analyzed *via* the $2^{-\Delta\Delta Ct}$ method (95), using *Tbp* (Mm00446973_m1) as a housekeeping gene.

Protein Extraction and Immunoblots

Mouse cervicothoracic spinal cord tissues (5 WT *versus* 5 KIN) were homogenized with a motor pestle in 5 to 10× weight/volume amount of radioimmunoprecipitation assay buffer consisting of 50 mM Tris–HCl (pH 8.0), 150 mM NaCl, 2 mM EDTA, 1% Igepal CA-630 (Sigma–Aldrich), 0.5% sodium deoxycholate, 0.1% SDS, cOmplete Protease Inhibitor Cocktail (Roche), and Halt Phosphatase Inhibitor Cocktail (Thermo Fisher Scientific, Inc). Similarly, MEF (3 WT *versus* 3 KIN lines) and human skin fibroblast (3 patients *versus* 3 controls) pellets were homogenized in radioimmunoprecipitation assay buffer by pipetting. The resulting protein suspensions were sonicated, and protein concentration was determined in a Tecan Spark plate reader (Tecan Group Ltd) using a Pierce BCA protein assay kit (Thermo Fisher Scientific, Inc). Total proteins (15–25 μg) were mixed with 2× loading buffer consisting of 250 mM Tris–HCl (pH 7.4), 20% glycerol, 4% SDS, 10% 2-mercaptoethanol, and 0.005% bromophenol blue, incubated at 90 °C for 5 min, separated on 8% to 15% polyacrylamide gels at 120 V, and transferred to nitrocellulose membranes (0.2 μm) (Bio-Rad Laboratories, Inc). The nitrocellulose membranes were blocked in 5% bovine serum albumin/Tris-buffered saline with Tween-20 and incubated overnight at 4 °C with primary antibodies. Afterward, the nitrocellulose membranes were incubated for 1 h at room temperature with fluorescently labeled secondary IRDye 800CW goat anti-mouse (LI-COR; catalog no.: 926-32210, 1:10,000 dilution), IRDye 800CW goat anti-rabbit (LI-COR; catalog no.: 926-32211, 1:10,000 dilution), IRDye 680RD goat anti-mouse (LI-COR; catalog no.: 926-68070, 1:10,000 dilution), or IRDye 680RD goat anti-rabbit (LI-COR; catalog no.: 926-68071, 1:10,000 dilution). Membranes were scanned using an Odyssey Classic Imager. Image visualization and quantification of signal intensities were performed using Image Studio software (version 5.2) (LI-COR Biosciences, Ltd). The following primary antibodies were used: ATXN2 (Proteintech; catalog no.: 21776-1-AP, 1:1000 dilution), BNIP3 (Proteintech; catalog no.: 68091-1-Ig, 1:1000 dilution), CTSB (Abcam; catalog no.: ab214428, 1:1000 dilution), LC3 A/B (Cell Signaling; catalog no.: 4108, 1:1000 dilution), NBR1 (Cell Signaling; catalog no.: 9891, 1:500 dilution), OPTN (optineurin; Proteintech; catalog no.: 10837-1-AP, 1:1000 dilution), PPIA (Proteintech; catalog no.; 10720-1-AP, 1:1000 dilution), SQSTM1/p62 (Cell Signaling; catalog no.: 39749, 1:1000 dilution), TAX1BP1 (Proteintech; catalog no.: 14424-1-AP, 1:1000 dilution), UBQLN2 (ubiquilin-2; Novus Biologicals; catalog no.: NBP2-25164, 1:1000 dilution), WDFY3 (Proteintech; catalog no.: 55009-1-AP, 1:1000 dilution), and WNK1 (protein kinase with no lysine 1; Invitrogen; catalog no.: PA5-28382, 1:1000 dilution). ACTB (Sigma; catalog no.: A5441, 1:10,000 dilution) or GAPDH (Calbiochem; catalog no.: CB1001, 1:10,000 dilution) served as loading controls.

Triple Immunofluorescence

Mouse spinal cord immunohistochemistry was performed as previously described (81). Here, the primary antibodies used were ATXN2 (BD Transduction; catalog no.: 611378, 1:50 dilution), PABPC1 (Abcam; catalog no.: ab21060, 1:100 dilution), SQSTM1 (Santa Cruz; catalog no.: sc25575, 1:50 dilution), and VIM (Calbiochem; catalog no.: LN6 clone V-9, 1:100 dilution). Secondary antibodies used were Alexa Fluor 488 goat anti-mouse IgG A11029, Alexa Fluor 488 goat anti-rabbit IgG A11034, Alexa Fluor 565 rabbit anti-goat IgG A11079, Alexa Fluor 568 donkey anti-sheep IgG A21099, and Alexa Fluor 568 goat anti-rabbit IgG A11036 (all Invitrogen, 1:1000 dilution).

Bioinformatics Analyses

STRING (search tool for the retrieval of interacting genes) webserver (https://string-db.org/) (version 11.0, last accessed on March 4, 2024) (96) was employed for the generation, visualization, and analysis of protein–protein interaction networks, using the list of proteins with dysregulated phosphorylations identified in the *Atxn2*-CAG100-KIN 14-month-old mice spinal cord phosphorylation profiling as input. Connectivity scores and interactions between the proteins were extracted as tab-delimited text files. The pathway enrichment analyses were conducted using different functional classification frameworks, including Gene Ontology, Kyoto Encyclopedia of Genes and Genomes Pathways, Reactome Pathways, and the Mammalian Phenotype Ontology (Monarch).

Disordered domains within ATXN2 and SQSTM1 were predicted using metapredict V2 (v2.4) (https://metapredict.net/, last accessed on February 29, 2024).

Phosphosites and their regulation in mice and humans according to the previously published literature were interrogated with the help of the database at www.phosphositeplus.org (last accessed on February 28, 2024).

Statistical Analyses

Unpaired Student's *t* tests with Welch's correction were used to establish comparisons for continuous variables between homozygous *Atxn2*-CAG100-KIN and WT animals. Treatments with bafilomycin were analyzed using two-way ANOVA. Bar charts depicting the mean and SEM values were used for data visualization. All statistical analyses were conducted using GraphPad Prism software (version 8.4.2) (GraphPad Software, Inc). Significance was assumed at $p < 0.05$ and highlighted with *asterisks*: Trend (T) <0.01; *$p < 0.05$, **$p < 0.01$, ***$p < 0.001$, and ****$p < 0.0001$.

RESULTS

Phosphoproteome Profile of End-Stage Spinal Cord from Authentic SCA2–ALS13 Mouse Model

Analyzing biological replicates of four WT *versus* four *Atxn2*-CAG100-KIN spinal cord tissues from 14-month-old mice, Fe-IMAC phosphorylation profiling detected a total of 80,278 redundant modified peptide assignments to 27,105 modified sites and documented 428 significantly downregulated *versus* 552 significantly upregulated phosphopeptides with at least two-fold changes (Supplemental Table S1, *A–E*).

Upon their analysis with the STRING webserver (Supplemental Table S1*F*), enrichments of pathways and Gene Ontology terms were observed, with significances

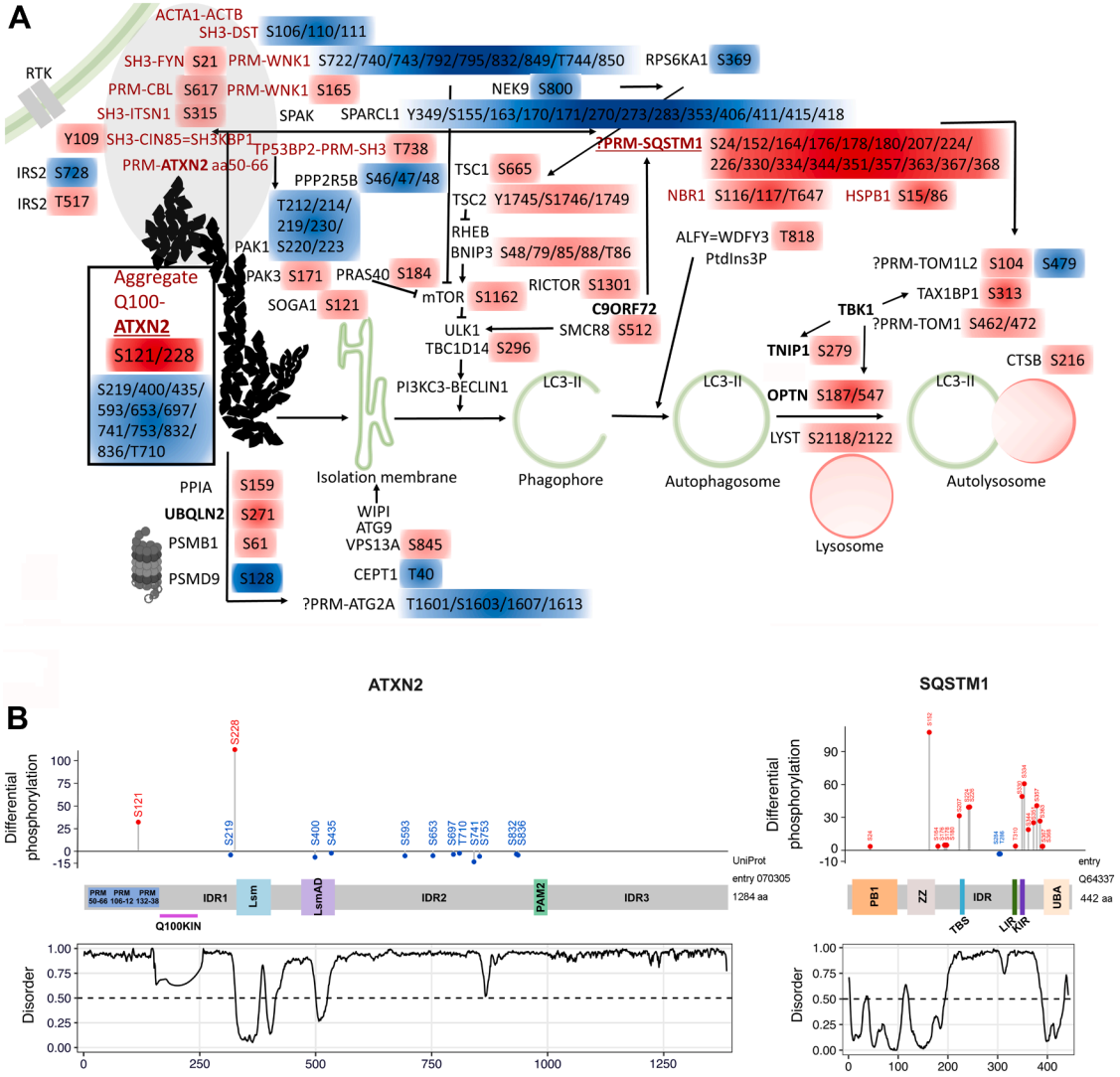

FIG. 1. **Main phosphoproteome findings.** *A*, schematic summary of phosphoregulation events of proteolysis and aggrephagy in the terminal-stage spinal cord of the *Atxn2*-CAG100-KIN mouse model of SCA2–ALS13. The potential coaggregation of ATXN2 (*black clusters*) with SH3-containing interactors and competing PRM-containing proteins that show differential phosphorylation is highlighted in a field with a *gray background*. Proteins potentially undergoing LLPS are highlighted in *red letters*, ALS disease proteins in *bold letters*. *B*, schematic protein structures and Q100-ATXN2-triggered differential phosphorylation events for ATXN2 as aggregating disease protein and for SQSTM1 as the main selective aggrephagy receptor, illustrating that massive hyperphosphorylations are flanking the Q100-KIN mutation replacing murine residue Q156 (*purple line*) and the three PRMs (*deep blue square*, with mouse residue numbers) in the N terminus of ATXN2, and are targeting the ZZ (*light gray square*) and LIR (*deep green column*) domains of SQSTM1. Hypophosphorylations across remaining ATXN2 likely reflect its reduced abundance upon polyQ expansion. The numbering of residues adheres to UniProt reference sequences, ignoring the unstable polyQ repeat KIN in ATXN2. Proteins are represented by their gene symbols, phosphorylated residue numbers are shown for serine (S), threonine (T), or tyrosine (Y). ALS, amyotrophic lateral sclerosis; ATXN2, ataxin-2; IDR, intrinsically disordered region, prone to phase separation; KIR, Keap1-interacting region; LIR, LC3-interacting region; LLPS, liquid–liquid phase separation; PB1, Phox and Bem1p; PolyQ, polyglutamine; PRM, proline-rich motif; PtdIns3P, phosphatidylinositol 3-phosphate; RTK, receptor tyrosine kinase; SCA2, spinocerebellar ataxia type 2; SH3, SRC-homology domain type 3; TBS, TRAF6-binding sequence; UBA, ubiquitin-associated; ZZ, zinc finger domain.

among the hyperphosphorylations for autophagy, ubiquitin, proteasome, ALS, and synapses (scheme of autophagy phosphoregulation in Fig. 1A and Supplemental Table S1*G*), whereas additional enrichments among hypophosphorylations for ion channels, glutamate neurotransmission, and myelin factors presumably reflected selective neuron loss.

As the key result, the ATXN2 N terminus with its polyQ expansion and three presumptive PRMs (UniProt entry: O70305 residues 50–66, 106–12, and 132–38) exhibited two massive hyperphosphorylations (112-fold at Ser228, 32-fold at Ser121). In phosphoproteome MS databases, we found no previous reports of phosphorylation or hyperphosphorylation at these residues, so they differ from known signaling cascades. Thus, they probably represent efforts to prevent phase separation and reflect the progressive neurotoxic ATXN2 gain-of-function in SCA2–ALS13. Similarly, massive hyperphosphorylations were observed only in the zinc finger domain (ZZ) and LC3-interacting region (LIR) domains of the aggrephagy receptor SQSTM1 (Fig. 1*B*). Conversely, 11 hypophosphorylations (at least twofold) across ATXN2 from the LSm domain to C-terminus (Fig. 1*B*) correspond to the known reduced abundance of Q100-ATXN2 in KIN nervous tissue because of impaired transcription/translation (77). They likely reflect the initial partial ATXN2 loss-of-function phenotypes in SCA2.

Among all hyperphosphorylation events, enrichment of SMART protein motifs by STRING analysis revealed SH3 domains to be strongly overrepresented with an FDR of $4.09e^{-08}$, including hyperphosphorylation of known ATXN2 interactors, such as CIN85 and ITSN1 (65, 67, 68). This finding is meaningful since it is reminiscent of the well-studied pathology in Huntington's disease (HD). PolyQ expansion in the N-terminus of the Huntingtin protein triggers adjacent PRMs to change conformation, phase separation, and interactions with SH3 proteins, thus acquiring neurotoxic properties (97–102). In analogy, the multipronged mutation effect in SCA2–ALS13 can be mediated by the massively hyperphosphorylated N-terminus of ATXN2, where the expanded polyQ domain is flanked by PRMs, which are known to interact with SH3 domains in the RTK–actin pathways. In contrast, the consistent hypophosphorylations across the ATXN2 central regions and the C-terminus with RNA-processing domains and intrinsically disordered regions (IDRs) (103), which control liquid–liquid phase separation (LLPS), would reflect the relative irrelevance of these ATXN2 areas.

Detailed Analysis of Pathway Enrichments for SH3 Domains and for Autophagy Factors

If both HD and SCA2 are mediated by aberrant associations of the PRMs in the disease proteins with specific SH3-containing targets, then the current data provide a unique insight to identify the interactor proteins primarily affected by the mutation, as well as PRM-containing proteins that compete with the disease protein for SH3 binding. In HD, only preliminary evidence *via* recombinant protein interactions exists that the PRM in Huntingtin can bind to SH3GL3, PACSIN1, and HYPA, but there are no data on endogenous proteins and how the enormous variety of SH3 sequences ranks in the power to modify disease progression (97, 101, 104). Now differential phosphorylation was documented, as listed in Supplemental Table S1, *I–L*, firstly for 28 SH3 domain–containing endogenous proteins (*e.g.*, hyperphosphorylations at a Tyr residue for ATXN2-interactor CIN85 aka SH3KBP1, and at different Ser residues for CIN85 and ITSN1 as endosomal regulators, for TP53BP2 as an autophagy modulator, for postsynaptic SHANK1, and for the tyrosine kinase FYN as regulators of glutamatergic neurotransmission and myelination, *versus* hypophosphorylations for DST as an autophagosome transport factor).

Differential phosphorylation was secondly noted also for 40 endogenous proteins with functionally studied PRM (like some hyper- and many strong hypophosphorylations of WNK1 as an autophagy modulator) and for 50 proteins with candidate PRM sequences near their dysregulated phosphosites (Supplemental Table S1*K*, including the hyperphosphorylations in SQSTM1), which have the potential to enter into aberrant competition with PRMs of ATXN2. This is very relevant for aggrephagy because the interactions of PRMs with SH3 domains are a classical driver of LLPS that promotes protein aggregation (105–111).

To search for coincidence pairs, where both an SH3-containing interactor and a potential PRM-containing competitor of ATXN2 are differentially phosphorylated, we first established which sequences in ATXN2 conform with the 10 established subtypes of PRMs (Fig. 1 in (112)), filtered all phosphoproteome data for experimentally confirmed PRM–SH3 interactions, and showed the resulting association chains in Figure 2. The most N-terminal ATXN2 PRM (murine amino acids [aa] 50–66, human aa 55–71) fitted the sequence constraints to explain interaction with almost all SH3 domains with differential phosphorylation, and another N-terminal ATXN2 PRM (murine aa 132–138, human aa 142–148) explained the NCF2–CYBA interaction. Thus, differential phosphorylation in direct interactor chains *via* PRM–SH3–PRM bridges may reflect the selective impact of Q100-ATXN2 on glutamatergic postsynapses (SHANK1, GRM1), myelination (FYN, MBP), and autophagy (WNK1).

The prominent 7.2-fold hyperphosphorylation of tyrosine kinase FYN (whose SH3 motifs would interact with ATXN2 PRMs in analogy to SRC as its family member (65, 67)) can influence endosome dynamics, nutrient uptake, and axon myelination (with strongly hyperphosphorylated BCAS1 and hypophosphorylated MBP/MAG/MOBP), conspiring with hyperphosphorylations of TSC2 to control mTORC1 signals, autophagy initiation, and cell growth (113, 114). This is the same pathway where ULK1 and ALS protein C9ORF72 were found to synergize with ATXN2 (115–117).

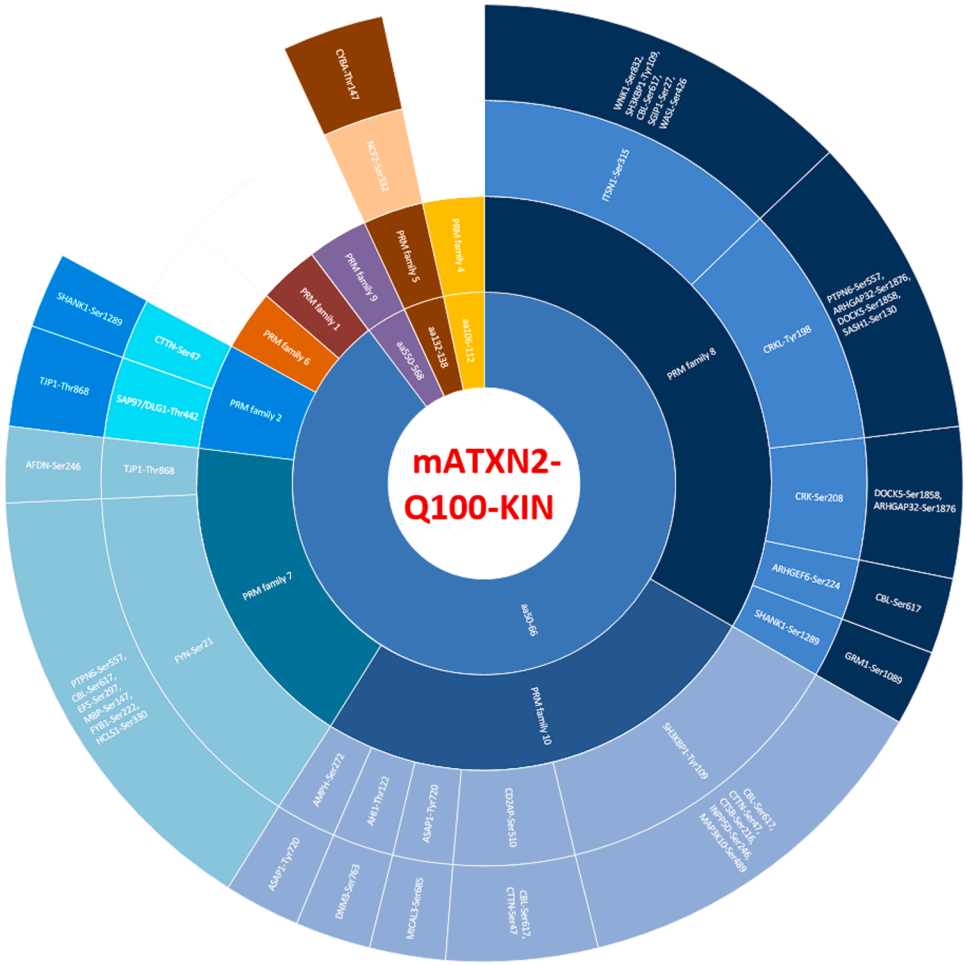

FIG. 2. **Synopsis of differentially phosphorylated PRM-containing and SH3-containing proteins, in their experimentally verified interactions according to the current literature, and in their binding to subtypes of PRM sequences within human ATXN2.** In this sunburst diagram, the outer ring shows PRM-containing differentially phosphorylated proteins that may compete with ATXN2 for SH3 binding. At appropriate positions in the ring below, their established SH3-containing interactors are shown with their phosphorylation changes. In the middle ring, the respective family of PRM sequences is shown that would bind to each SH3-containing protein. Inner rings illustrate which N-terminal ATXN2 sequences correspond to these PRM families and could therefore compete with the PRM-containing proteins in the outer ring for their SH3 associations. Within ATXN2, the PRM at murine residues 50 to 66 has a complex pattern of prolines that can interact with diverse SH3 domains, such as PRM subtypes 2 (may impair, *e.g.*, CTTN binding to SHANK1), 7 (may impair FYN binding to FYB1 and MBP and PTPN6), 8 (may impair CIN85/SH3KBP1 binding to CBL), and 10 (may impair SHANK1 binding to GRM1 and also ITSN1 binding to WNK1). ATXN2, ataxin-2; PRM, proline-rich motif; SH3, SRC-homology domain type 3.

Differential phosphorylation was third encountered at tyrosine residues in 26 proteins, and indeed the tyrosine phosphatase PTPN6 showed a 2.1-fold pSer557 change. These observations suggest trophic signaling at RTKs to be altered (like 2.6-fold pTyr1745-TSC2 as mTOR repressor, 4.0-fold pTyr3363-ANK2 as an actin adaptor in motor neurons, or 4.6-fold pTyr47-NDRG2 as a neuronal differentiation factor) (Supplemental Table S1, *I*–*L*).

As a final and crucial result of STRING enrichment statistics, the PB1 domains that mediate multimerization of SARs were over-represented (FDR 0.0159), so these receptors were studied in detail later.

Among the top 30 hyperphosphorylations (>7-fold), the ALS disease proteins ATXN2, SQSTM1, UBQLN2, OPTN, and TBK1-regulated TAX1BP1 stood out (compared with the ALS protein TNIP1 [TNFAIP3 interacting protein 1] with 2.7-fold hyperphosphorylation, Table 1 and Supplemental Table S1*H*). This was in overlap with four SARs that mediate (118, 119) aggrephagy, lysophagy, pexophagy, and granulophagy (SQSTM1, NBR1, and TAX1BP1; further, WDFY3 showed a 3.2-fold increase, Supplemental Table S1*E*) as well as mitophagy (OPTN; with four peptides from BNIP3 showing 2.4–2.2-fold increases). Further proteostasis factors among the top 30 hyperphosphorylations included the proteasomal

TABLE 1

List of the strongest hyperphosphorylations in KIN spinal cord (changes above sevenfold, showing aggregating disease protein in underlined letters, proteostasis factors in bold letters, and actin-/myelin-associated factors italicized)

Normalized fold change	*p*	Protein name	Phosphosite	PubMed ID		
ATXN2: WT	ATXN2: WT			Literature autophagy	Literature SCA–ALS	Literature actin
112.2	0.00	ATXN2	228; 228; 228	38308810, 30982600	8896555, 28405022	12524342, 34977501
107.6	0.00	**SQSTM1**	§152; §152	22736434, 33332721	20301623, 35143965	25015291
66.2	0.00	**PSMB1**	§61	36602366	—	—
60.9	0.00	*CDR2L*	§344	—	36729270	19427213, 19602412
60.7	0.00	**SQSTM1**	§330, §334, 344; §330, §334, 344	31585693	30657305, 35143965	25015291
50.2	0.00	*ANK2*	§909; §914; §914; 860; 76	35226578	29078305	25533844, 29163198
49.1	0.00	**SQSTM1**	§330, 344; §330, 344	22736434, 33332721	30657305, 35143965	25015291
49.1	0.00	**SQSTM1**	§334, 344; §334, 344	22736434, 33332721	30657305, 35143965	25015291
47.4	0.00	*BCAS1*	§443	—	—	16133941, 29212715
40.7	0.00	**SQSTM1**	§357, §363, §368	22736434, 33332721	30657305, 35143965	25015291
39.3	0.00	**SQSTM1**	§226; §226	22736434, 33332721	30657305, 35143965	25015291
39.3	0.00	**SQSTM1**	224; 224	22736434, 33332721	30657305, 35143965	25015291
39.2	0.00	**SQSTM1**	§357, §363, §367	22736434, 33332721	30657305, 35143965	25015291
32.2	0.00	ATXN2	121; 121; 121	38308810, 30982600	8896555, 28405022	12524342, 34977501
31.5	0.01	**SQSTM1**	§207; §207	22736434, 33332721	30657305, 35143965	25015291
26.7	0.00	**SQSTM1**	§363, §368	22736434, 33332721	30657305, 35143965	25015291
25.2	0.00	**SQSTM1**	§351, §363, §368	22736434, 33332721	30657305, 35143965	25015291
18.4	0.00	**SQSTM1**	344; 344	22736434, 33332721	30657305, 35143965	25015291
17.8	0.03	*PDHA1*	§295, §300	35731579	20002125, 37422902	—
17.2	0.00	**UBQLN2**	271	35708843	25398946, 30442662	23635659, 24549040
16.6	0.00	**ARID1A**	§1601; 1384; 1221; 1220	36229854	28662958	25195934, 38017409
14.6	0.00	**UBQLN2**	§267, 271	35708843	25398946, 30442662	23635659, 24549040
10.9	0.00	**CYBA**	§147; 119	33138004	23830905	16341922
10.7	0.00	**TAX1BP1**	§313	35470757, 33207181	—	29398621
10.0	0.02	**OPTN**	§547	29867991, 33783320	20428114, 38178841	23781020, 29875258
9.8	0.00	**NBR1**	§117	21189453, 36255390	27551461, 31362587	—
8.7	0.03	**CTSB**	216	30107168	32757690	23018451
8.3	0.00	**SPP1**	§283, §290	21374592, 36505285, 38082480	36460480	10842093, 34576260
7.3	0.00	*CDH10*	§784	35721483	31176720	29030434
7.2	0.00	**FYN**	§21; §21	22745922	28935570, 30154836	10224664, 28887403

subunit PSMB1, the lysosomal peptidase CTSB, and the LC3-dependent phagocytosis factor CYBA (120, 121) (Table 1). Particularly strong reductions of phosphorylation were documented in WNK1 (fold change −7.1) and in NEK9 (fold change −3.8), an adaptor for actomyosin autophagy in cooperation with MYH9 (122–124), suggesting cytoskeletal affection.

A unique, truly extraordinary hyperphosphorylation (107.6-fold) at Ser152-SQSTM1 was observed at the ZZ domain (Fig. 1) as the cargo recognition motif for N-term-arginylated proteins, whose target association facilitates disulfide bond–linked multimerization and LC3-mediated autophagosome binding (125, 126). This finding suggests an activation of arginyltransferase-1 to facilitate autophagic removal of polyQ-expanded ATXN2 *via* SQSTM1, as described for endoplasmic reticulum (ER) phagy (127, 128). Also, actin assembly rates in linear and branched networks are modified by N-terminal arginylation (129, 130). Indeed, arginyltransferase-1 showed significant hyperphosphorylation in the present dataset.

In contrast, a striking paucity of RNPs was apparent among all altered phosphosites (except ATXN2, with small changes for DCP1A, DDX3, EDC3, EDC4, PCBP1, PRKRA, RPS6KA1, SLIRP, SRRM1, SRSF6, SRSF9, and TRIR), conspicuously showing no change for TDP-43, FUS, C9ORF72, TBK1, SOD1, or other ALS1–28 disease proteins. This may either suggest that RNP functions are not much affected or that these factors are differently regulated, for example, by arginine methylation rather than by phosphorylation.

Levels of Protein Abundance and mRNA Expression for Dysregulated Autophagy Factors in End-Stage Spinal Cord From Atxn2-*CAG100-KIN Mice*

The phosphochanges affected an individual residue, for example, in the case of ATXN2L, TAX1BP1, PPIA, CTSB, and WDFY3 (Supplemental Fig. S1). However, ATXN2, SQSTM1, NBR1, as well as OPTN, SPARCL1 (secreted protein acidic and cysteine rich-like 1), UBQLN2, BNIP3, and WNK1 showed similar dysregulations across several domains (Fig. 1 and Supplemental Fig. S1). Therefore, it was important to assess (at least for key regulators) the overall protein abundance and transcript levels. Quantitative immunoblots of the KIN spinal cord tissue showed elevated abundance for SQSTM1, NBR1, BNIP3, WDFY3, CTSB, PPIA, and TAX1BP1, but only the *Sqstm1* and *Ctsb* mRNA were increased upon RT–qPCR (Fig. 3 and Supplemental Figs. S2, S3). UBQLN2 abundance was unchanged (Supplemental Fig. S3). There was no specific and sensitive antibody to detect endogenous WNK1 available to us. Despite the increase of its two phosphosites, OPTN protein abundance was diminished, and its mRNA levels were unchanged (Fig. 3). Thus, these selective hyperphosphorylation events appear to reflect true cellular signaling efforts. This includes the 10.0-fold increase of pSer547, which is close to the C-terminal region (that binds MYO6 [unconventional myosin VI] and TAX1 in competition with TAX1BP1 (131–133)) and its polyubiquitin binding ZF motif (134). These meaningful OPTN hyperphosphorylations also include the 2.7-fold increase of pSer187 within the LIR domain, which regulates the binding to autophagosome membranes. Analysis of the MYO6 abundance in the KIN spinal cord showed significantly elevated levels, but the *Myo6* mRNA was decreased (Fig. 3). This putative transcriptional compensation suggests the accumulation of autophagosome fusion factor MYO6 to be pathological. Consistent with its many decreased phosphosites, SPARCL1 protein abundance and *Sparcl1* mRNA levels were reduced (Fig. 3). SPARCL1 is an extracellular factor that promotes excitatory synaptogenesis as a member of a protein family that controls autophagy and apoptosis (135, 136). Transcript decreases were also observed for *Bnip3*, *Wdfy3*, *Ppia*, and *Tax1bp1*, suggesting that the encoded proteins have aberrantly slowed turnover and that the accumulation of the encoded proteins has a pathological effect leading to compensatory transcriptional downregulation. Unchanged levels were documented for *Ubqln2* and *Wnk1* (Supplemental Fig. S2).

Overall, this study of spinal cord tissue in our SCA2–ALS13 mouse model documented massive inductions for SQSTM1 and NBR1 proteins, which are known to accumulate in TDP-43 aggregates upon ALS-associated mutations (137–141). Conversely, our spinal cord study observed a loss-of-function of OPTN where autosomal recessive mutations are known to cause ALS type 12 (142–147). Subsequent analyses of autophagy mechanisms *in vitro* focused on the regulation of these factors.

Interestingly, the induction of SQSTM1 protein was >5-fold. This suggests that several increases of phosphopeptides in SQSTM1 can be explained by higher protein abundance; only the extraordinary increase at pSer152 near the ZZ domain, with the strong increases at residues 207 to 226 around the TRAF6-binding sequence (TBS), as well as residues 330 to 363 around LIR and Keap1-interacting region (KIR) reflect selective phosphorylation efforts. The *Sqstm1* mRNA was induced only <1.5-fold, indicating that multiple translation rounds occur to amplify SQSTM1 availability.

Mechanistically asking whether ATXN2 as a factor known to influence mRNA stability and translation efficiency has a selective impact on this event, we interrogated previously published data (57) on the identity of mRNAs that are bound directly by ATXN2. As shown in Supplemental Fig. S4, a specific interaction of ATXN2 to *Sqstm1* transcript was reported in its 3′UTR, overlapping with sequences binding to the RNA helicase DDX6 and with an interaction site for miR-183-5p. This microRNA is known to regulate the levels of SQSTM1 and to have abnormal levels in ALS (148, 149). Thus, ATXN2 can influence the levels of SQSTM1 protein *via* a PRM–SH3 bridge and the stability/translation of *Sqstm1* mRNA *via* its 3′UTR.

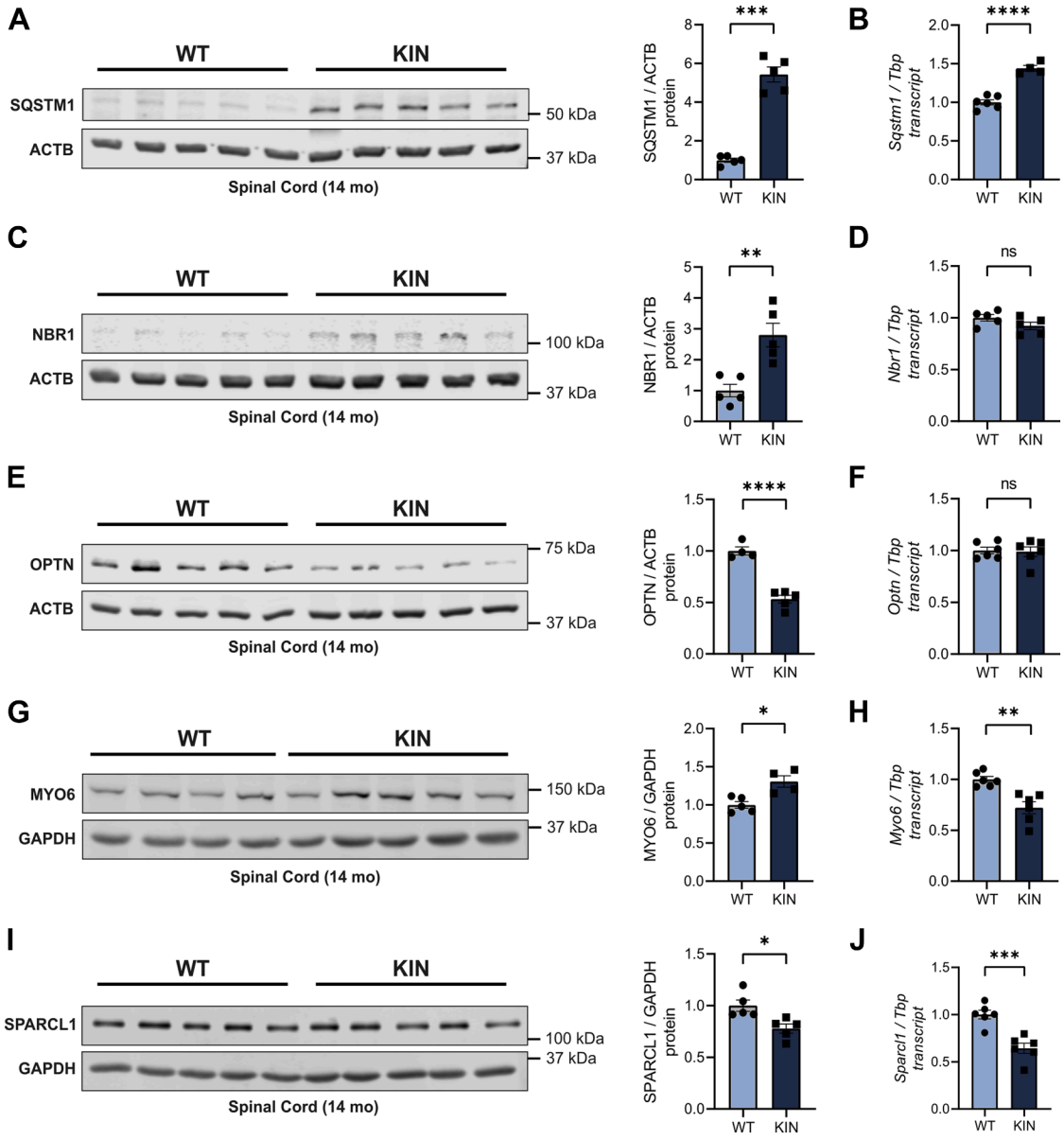

FIG. 3. **Quantitative immunoblots (*A*, *C*, *E*, *G*, *I*, N = 5 or 4 *versus* 5) and quantitative reverse-transcriptase real-time PCR (*B*, *D*, *F*, *H*, *J*, N = 6 *versus* 6) for SQSTM1 (*A*, *B*), NBR1 (*C*, *D*), and OPTN (*E*, *F*) as main aggrephagy receptors, as well as MYO6 (*G*, *H*) and SPARCL1 (*I*, *J*) in end-stage spinal cord from our SCA2–ALS13 mouse model *Atxn2*-CAG100-KnockIn (KIN) *versus* WT.** SQSTM1 and NBR1 were chosen in view of their hyperphosphorylated peptides, OPTN in view of its mix of hyperphosphorylations and hypophosphorylations, together with its interactor MYO6, and SPARCL1 in view of its many hypophosphorylated peptides. The protein changes are reflected by similar transcript upregulation for SQSTM1, *versus* downregulation for SPARCL1, but the MYO6 protein accumulation is counteracted by down-regulation of *Myo6* mRNA—a possible correlate of deficient autophagosome fusion with lysosomes. *$p < 0.05$; **$p < 0.01$, ***$p < 0.001$, and ****$p < 0.0001$, ns, not significant. ALS, amotrophic lateral sclerosis; MYO6, unconventional myosin VI; OPTN, optineurin; SCA2, spinocerebellar ataxia type 2; SPARCL1, secreted protein acidic and cysteine rich-like 1.

Regulation of Autophagy Factors Upon BafA1 and NaARS Administration in Embryonic Fibroblasts From Atxn2-CAG100-KIN Mice and Skin Fibroblasts From SCA2 Patients

Fibroblasts from the mouse model and SCA2 patients were used to test whether the regulation of autophagy factors in response to stressors is altered by ATXN2–polyQ expansions, using alternatively the drug BafA1 that inhibits autophagy by interference with lysosome acidification (150) or the drug NaARS that triggers protein misfolding *via* oxidative stress and thus promotes stress granule formation in parallel to protein breakdown (151).

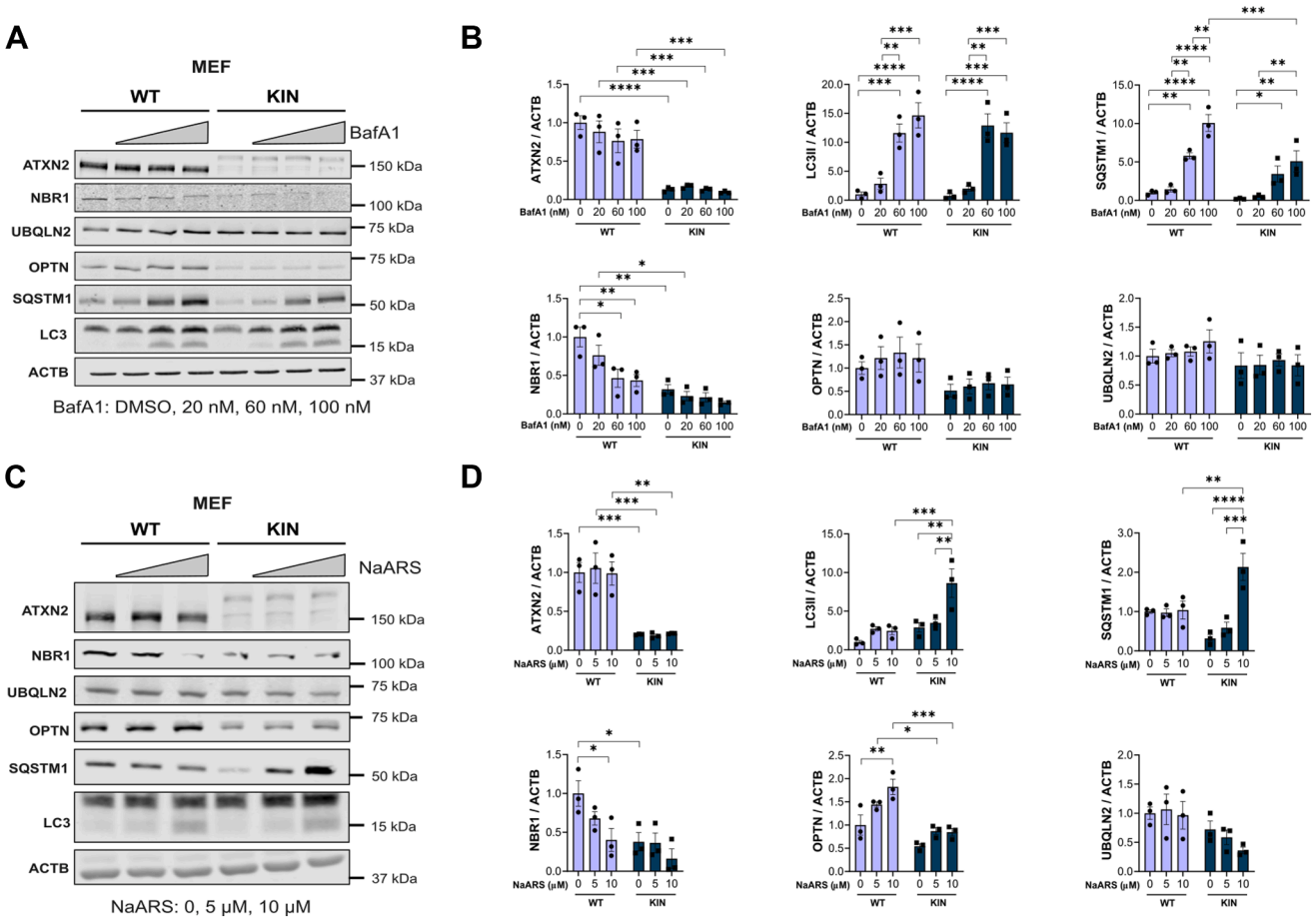

FIG 4. **Quantitative immunoblots of autophagy factors in *Atxn2*-CAG100-KIN *versus* WT MEF (N = 3 *versus* 3) treated at increasing dosage either (*A, B*) with the lysosomal toxin bafilomycin A1 (BafA1) or (*C, D*) with the oxidative stressor sodium arsenite (NaARS).** *$p < 0.05$; **$p < 0.01$, ***$p < 0.001$, and ****$p < 0.0001$. KIN, knockin; MEF, mouse embryonic fibroblast.

The interference with autophagic degradation by BafA1 treatment showed the following effects in MEFs: It impaired autophagic flux as detected by LC3-II accumulation at higher dosages both in WT and mutant cells, but the KIN cells showed consistently much lower soluble ATXN2 protein levels, impaired inducibility of SQSTM1 protein, and tendentially lower OPTN abundance (Fig. 4, *A* and *B*).

The generation of high autophagy demand by NaARS treatment generated overlapping effects: In WT MEF, it did not affect LC3-II or SQSTM1 levels, whereas NBR1 decreased and OPTN increased with dosage. In KIN MEF, NaARS caused accumulation of LC3-II (>8-fold) and SQSTM1 (>2-fold), whereas the abundance of NBR1 and OPTN showed genotype-dependent reductions (Fig. 4, *C* and *D*).

Overall, these data agree with the OPTN deficiency that was observed in the KIN spinal cord and suggest the SQSTM1 induction to be deficient in SCA2–ALS13. OPTN induction shows a smaller size than SQSTM1 induction, underscoring their differing importance for aggrephagy.

Next, three previously described SCA2 patient fibroblasts (polyQ expansions to CAG40/41/49, females with manifestation ages at 17–53 years (67)) *versus* sex-/age-matched controls were treated with BafA1. ATXN2 abundance exhibited almost normal levels in these human peripheral cells, presumably because the expansion sizes were much smaller than in the KIN MEF. The BafA1 treatment caused impaired autophagic flux as detected by more LC3-II abundance at higher drug dosage in both WT and mutant cells (less in SCA2). Selectively, the SCA2 cells showed the accumulation of soluble LC3-II and SQSTM1 proteins to be restricted at high dosage, as previously observed for LC3-II in ATXN2-Q58 KIN HEK293 cells (152), in parallel to higher NBR1 abundance and trends to elevated UBQLN2 abundance (Fig. 5, *A* and *B*). The findings may be explained by LC3-II and SQSTM1 becoming partially insoluble, indicating that autophagy problems contribute to the aggregation process. Importantly, these results are compatible with the aforementioned findings that autophagy problems are a primary consequence of

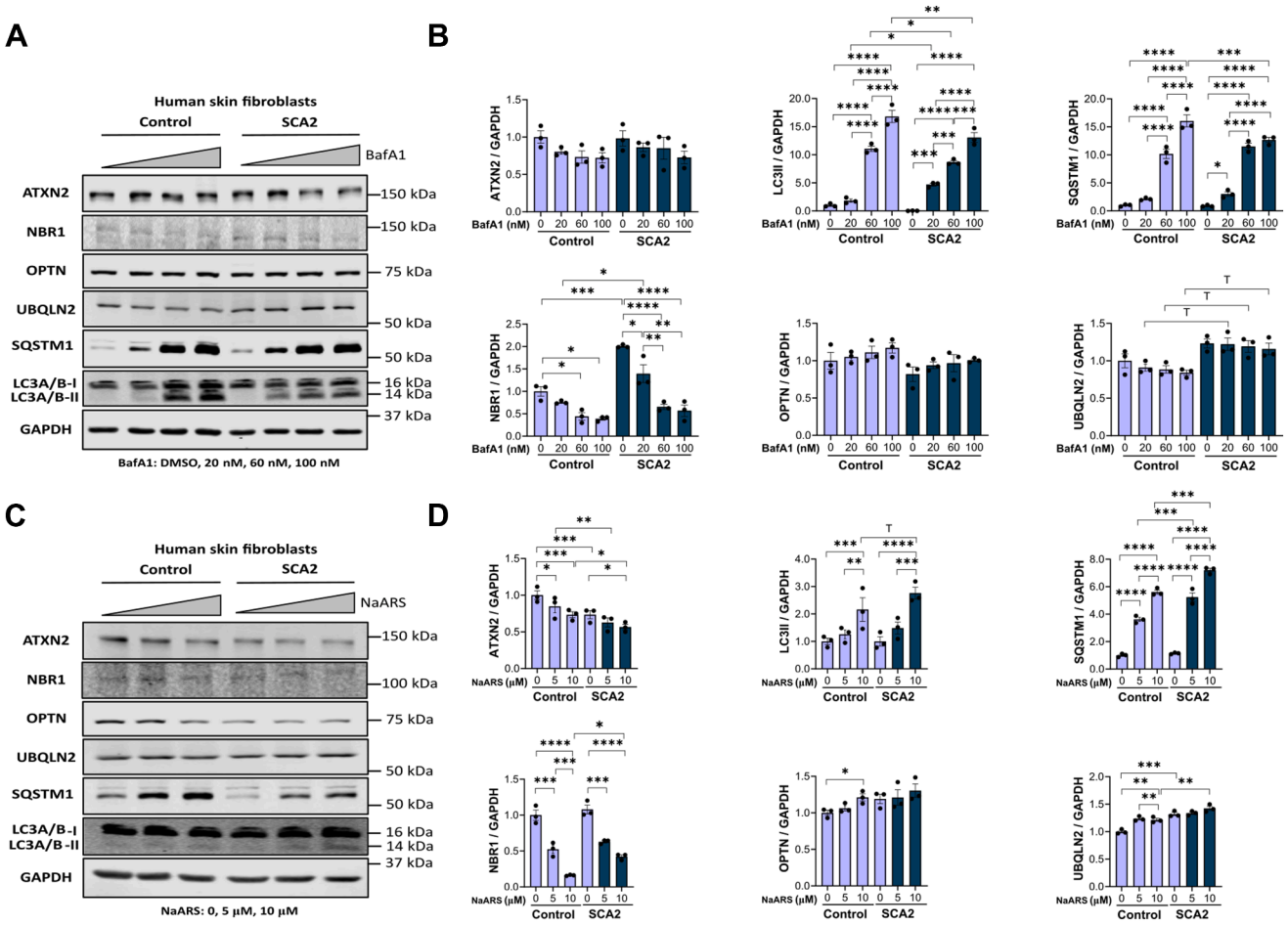

FIG. 5. **Quantitative immunoblots of autophagy factors in SCA2 patient skin fibroblasts (N = 3 mutants *versus* three controls) treated at increasing dosage either (*A, B*) with the lysosomal toxin bafilomycin A1 (BafA1) or (*C, D*) with the oxidative stressor sodium arsenite (NaARS).** T < 0.10; **p* < 0.05; ***p* < 0.01, ****p* < 0.001, and *****p* < 0.0001. SCA2, spinocerebellar ataxia type 2.

ATXN2 polyexpansion, *via* the mRNA stability and translation of SQSTM1. Furthermore, the data reveal cellular efforts in human SCA2 for a putative compensation *via* NBR1-dependent aggrephagy and UBQLN2-dependent ubiquitin/proteasome-mediated proteolysis.

Upon NaARS treatment of human skin fibroblasts with high demand for autophagic proteolysis, the accumulation of SQSTM1 and LC3-II was elevated in SCA2 patient cells, suggesting that the inducibility of SQSTM1 and LC3-II is not limited by the typical polyQ expansion sizes in most patients (Fig. 5, *C* and *D*). Again, compensatory increases of NBR1 and UBQLN2 were found.

It was interesting to note that aggrephagy appeared to enhance the need for SQSTM1 while lowering endogenous NBR1 levels, suggesting that they can represent alternative SAR options, an observation that contrasts with the mutual positive regulation of both factors reported during viral infection and for adenovirally transfected NBR1 (153, 154). Overall, both *in vitro* models of SCA2–ALS13 indicate that the polyQ expansion enhances the cellular need of SQSTM1 and autophagic flux upon oxidative stress but restricts the maximal availability of soluble SQSTM1 protein. These observations might be explained by LLPS of expanded ATXN2 with SQSTM1 into aggresomes, even in peripheral fibroblast cells.

Subcellular Localization of PolyQ-Expanded ATXN2- and SQSTM1-Positive Aggresomes in Atxn2*-CAG100-KIN Spinal Cord*

To characterize the aggresome formation in SCA2 by an additional approach, triple immunofluorescent immunohistochemistry was employed to document the cytoplasmic localization of ATXN2 and SQSTM1 in affected neurons of the spinal cord (Fig. 6), in comparison to PABPC1 as a known direct RNP interactor of ATXN2 (44, 50, 155). A previous publication already documented the sequestration of ATXN2 and TDP-43 to aggregates in spinal motor neurons of aged KIN mice (81). In the current study, SQSTM1 aggregates were

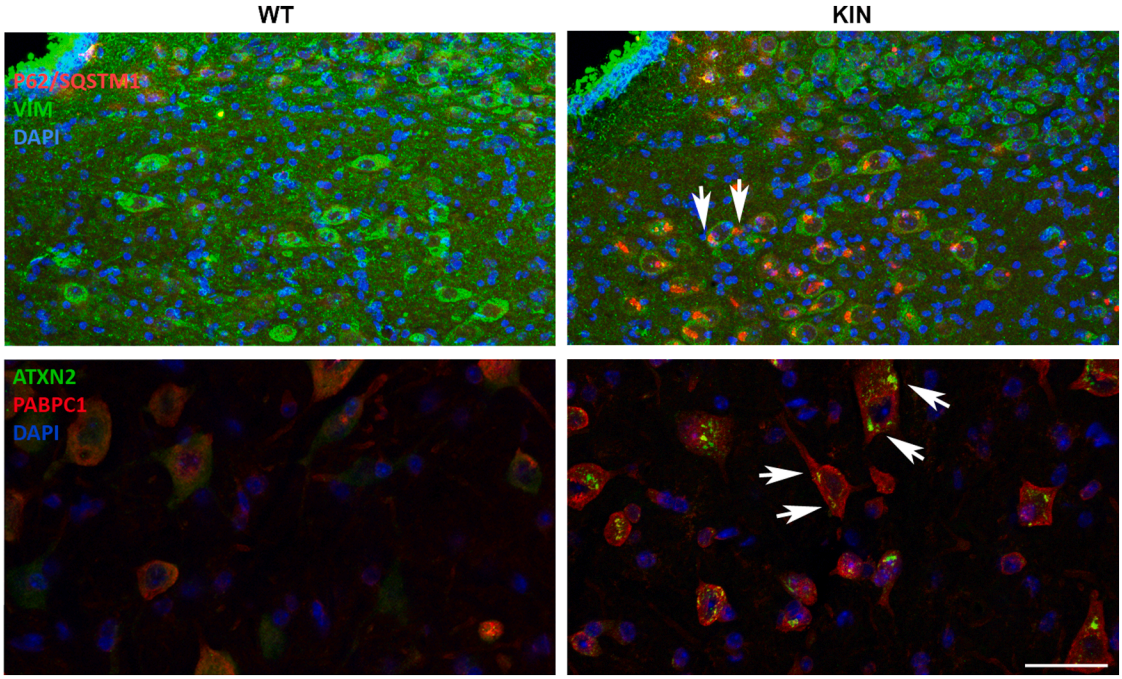

FIG. 6. **Triple immunofluorescent histochemistry by confocal laser scanning microscopy with composite panels from Z-stacks.** Detection was done for the selective autophagy receptor SQSTM1 and the ribonucleoprotein PABPC1, compared with intermediate filament vimentin (VIM) or ATXN2, and nuclear DAPI signals, in the spinal cord of old sex-/age-matched adult WT *versus Atxn2*-CAG100-KnockIn (KIN) mice. *White arrows* in the *upper row* point to SQSTM1 aggregates at opposite poles of the nucleus, where microtubule-organizing centers are expected to establish neuronal polarity and provide a starting point for axonal or dendritic transport. *White arrows* in the lower row point to ATXN2 aggregates at opposite poles of the nucleus. DAPI, 4′,6-diamidino-2-phenylindole; PABPC1, poly(A)-binding protein 1.

readily apparent in the motor neuron cytosol of KIN mice at opposite ends of the nucleus, where aggresomes form near microtubule-organizing centers (MTOC), as previously observed (156) (Fig. 6, *upper row*). While ATXN2 also showed aggregate formation at opposite ends of the nucleus in spinal motor neurons of KIN mice, PABPC1 staining showed mostly a diffuse cytoplasmic localization (Fig. 6, *lower row*). Thus, in KIN spinal cord motor neurons, the polyQ-expanded ATXN2 and SQSTM1 show enhanced transport *via* the cytoskeleton to MTOCs.

DISCUSSION

When protein aggregates cause neurodegenerative processes, it is little understood how cells adapt their signaling to mitigate the pathology, for example, by improving the solubility of phase-separated sequences or by modifying protein surfaces to control their interactions. Our authentic mouse model of SCA2–ALS13 with its strong phenotype offers an opportunity to document these molecular events between endogenous proteins in the selectively affected areas of the nervous system. As a key finding, the molecular scenario of SCA2–ALS13 mirrors the following six features that were already reported for the well-known polyQ expansion–driven neurodegenerative processes in autosomal dominant HD. In HD, 1) exon 1 of the Huntingtin gene drives pathogenesis, 2) erroneous splicing of this exon 1, and 3) abnormal proteolysis of the N-terminal fragment was observed in KIN mouse models and patient cells, 4) a PRM lies adjacent to the polyQ domain, 5) the abnormal interaction of this PRM with SH3 domains is responsible for the disease progression, and 6) exerts selective aggrephagy effects *via* OPTN and MYO6 (97–102, 104, 157–172).

In our study on SCA2–ALS13, a main finding is that the cellular phosphorylation responses to ATXN2 polyQ expansion appear massively and selectively upregulated within the N-terminus between residue Ser121 and Ser228. This observation indicates numerous important insights.

The N-Terminus of ATXN2 With Its PolyQ Repeat and Three PRMs Has a Decisive Role

The possibility exists that an N-terminal fragment of polyQ-expanded ATXN2 is generated by abnormal splicing, translation, or proteolysis, to then accumulate in postmitotic cells as a driver of LLPS and the neurotoxic aggregation process. This fragment may be too insoluble and too small for unequivocal detection in immunoblots (the corresponding efforts were unsuccessful in our hands) but may have been present in the MS (173). Consequently, the antibodies against the polyQ-expansion domain (such as 1C2) and the antibodies against these N-terminal ATXN2 sequences would detect the aggregates much better than the current

commercial antibodies raised against the remainder of ATXN2. Furthermore, it is crucial to consider how efficiently ASOs are targeting and completely degrading the 5′-terminal sequences of the ATXN2 mRNA for optimal prevention of the neurodegenerative process in SCA2–ALS patients.

As a result of alternative splicing (174), the main isoform of human ATXN2 begins with the sequence MSLKPQQQQ QQQQQQQQQQQQQQQQQQPPP (UniProt entry: A0A2R8Y5A6), and the RNA-binding LSm domain starts 80 residues further downstream. The minor isoform includes an additional 160 residues at the N-terminus (UniProt entry: Q99700), which contain three putative PRMs (first, aa 55–71 PPPPGPGPPPSRQSSPP, which appear to be responsible for most SH3 interactions according to Fig. 2 and Supplemental Table S1*L*; second, aa 117–123 PPAAPTR; third, aa 142–148 RPAPGCP, whose sequence would interact only with the SH3 protein NCF2 in competition with the PRM protein CYBA according to Supplemental Table S1*L*). Before the polyQ domain, before the LSM domain, and before the minor isoforrm at the N-terminus there are methionine residues providing 3 alternative translation start codons, with the 3 corresponding alternative isoforms being documented in the UniProt database. These sequences are highly conserved among mammals; in mouse, only aa 117 to 123 has a relevant change to PAATPAR (UniProt entry: O70305). This extended N-terminus does not exist in yeast, worms, flies, or zebrafish. During phylogenesis, the first N-terminal PRMs appeared in the ATXN2–ATXN2L ortholog of lizards (UniProt entry: A0A670IJW1). Given that interactions of ATXN2 with SH3 domains will influence the actomyosin cytoskeleton below cell membranes, the ATXN2 isoform with an extended N terminus may have developed to ensure RNA quality during long-distance trafficking along the dendrites of larger land animals and particularly in peripheral cell compartments like synapses. In the cell periphery, ATXN2 with an extended N-terminus and multiple SH3 interactions will also be more efficient in regulating the RTK-dependent endocytic uptake of nutrients, mTORC1 signaling, and stress/stimulus-dependent local translation. Thus, it will be impossible to faithfully model the diverse aspects of SCA2–ALS13 pathogenesis, for example, in yeast and flies, where the isoform with PRMs in the extended N-terminus does not exist.

Characteristic Features of SCA2–ALS13 Can Be Explained by Preferential Affection of SH3-PRM–Containing Proteins With Conspicuous Phosphorylation Changes

The neurotoxic gain-of-function appears to be determined by abnormal folding, binding, and solubility of the expanded polyQ domain and adjacent PRM domains of ATXN2 and its corresponding SH3 domain–containing interactor proteins, affecting the actomyosin cytoskeleton together with the motility of cell membranes, in particular RTK and nutrient endocytosis, as well as ribosomal translation, resulting in the progressive atrophy of the nervous system.

Indeed, polyQ-expanded ATXN2 triggers phosphorylation changes with significant enrichment among SH3 proteins, which modulate actin and endocytosis dynamics in the cell periphery as well as ribosomal translation, and which are credible correlates of the SCA2–ALS-typical neural atrophy pattern. The preferential affection of glutamatergic synapses between upper and lower motor neurons of the corticospinal projection, and between granule neuron axons known as parallel fibers and Purkinje neuron dendrites, could be explained by polyQ–ATXN2-triggered phase separation of SH3-containing proteins, for example, the hyperphosphorylated SHANK1 and the enhanced interactors, SHANK2 and DLG4 (discs large MAGUK scaffold protein 4; aka PSD-95) as postsynaptic components of excitatory synapses (175). LLPS of SHANK might underlie the tandem hypophosphorylations in the PRM-containing metabotropic glutamate receptor GRM1 (aka MGLUR1) as a main factor for dendritic spine biogenesis and as a disease protein responsible for autosomal recessive SCAR13 and autosomal dominant SCA44 (176, 177), and might also underlie the prominent multiple hypophosphorylations/reduced abundance of SPARCL1 as a factor responsible for the formation of excitatory synapses (113). An association with the pathogenesis of motor neuron disease was previously reported for SPARCL1 (aka Hevin) (136, 178, 179). The prominent downregulation of SPARCL1 in the present dataset, where spinal motor neurons are lost because of SCA2, and the implication of SPARCL1 in ALS are consistent with a recent report about single-cell sequencing efforts in the spinal cord that identified SPARCL1 mRNA among the top 50 transcripts enriched in spinal motor neurons (Fig. 6 in (180)). Also, the strong demyelination in SCA2 can be correlated to the hyperphosphorylation of the SH3-containing protein FYN as a main regulator of axon–oligodendroglia signaling (181) with its interactor protein FYB1–ADAP (182) and to adaptive, prominent, multiple hypophosphorylations in the PRM-containing myelin proteins MAG, MBP, and MOBP (183). As seen in Figure 2, many other interactions between SH3 and PRM proteins show mild hyperphosphorylations, suggesting they might be partially affected by the phase separation process, for example the SH3 proteins DLG1, CTTN, and TJP1/ZO-1, as well as the PRM proteins AFDN, PXN, VASP, and PAK3, as modulators of synaptic adhesion (184–190), or the SH3 protein NCF2 and the PRM protein CYBA, as mediators of microglial neuroinflammation (191).

A further combination of hyperphosphorylations in the SH3 proteins, ITSN1, SRC, SH3KBP1–CIN85, as endocytosis regulators, *versus* hypophosphorylations in the PRM protein ARHGAP32/PX-RIX as an endosome-associated factor (192) was observed for the nutrient uptake pathway that governs mTORC1 signaling and cell growth. Finally, the combination of hyperphosphorylation in the SH3 protein AHI1 as an endocytosis/autophagy modulator (193), as well as accumulation of the SH3 protein MYO6 as an autophagosome maturation factor (165), *versus* multiple prominent

hypophosphorylations/reduced abundance in the PRM-containing proteins (Supplemental Table S1*K*) was noteworthy. WNK1 as an autophagy regulator (194), ATG2A as an autophagy initiation factor (195), and TOM1L2 as a xenophagy mediator (196) also suggest these events to be among the primary erroneous protein interaction consequences upon polyQ expansion in ATXN2. The enhanced binding of Q100-ATXN2 to the ribosomal components RPL12 and the SH3-containing RPL21 (ribosomal protein large subunit component 21) may impair initiation, elongation, and fidelity of mRNA translation, thus contributing to the mTORC1 inhibition phenotype.

In view of the importance of PRM–SH3 interactions for the neurotoxicity of polyQ expansions in SCA2–ALS13, it should be noted that targeting the SH3-containing SRC protein and its signaling pathway was recently proposed to develop a preventive treatment of ALS (197).

Excess Autophagy May Be a Primary Direct Effect, Leading to SQSTM1 and OPTN Deficiency

Crucially in the case of polyQ-expanded ATXN2, the phosphoproteome suggests excessive autophagy in SCA2–ALS13 not to be an indirect late consequence in the course of disease but a primary autodestructive phenomenon that is triggered by abnormal competition between ATXN2–PRMs and SQSTM1–PRM and/or WNK1-PRMs for association with SH3-domain proteins such as MYO6 as autophagosome motor protein, ITSN1/CIN85/SRC in endocytosis, RPL21 in ribosomal translation, FYN in myelination, and SHANK1 in glutamatergic postsynapses. As previously shown, the recruitment of SH3-containing proteins into phase-separated sequestosomes reduces their biological activity and function, for example, in the case of SRC restricting the activation of PI3K and the formation of filopodia-like cell protrusions (198).

A direct effect of polyQ-expanded ATXN2 on autophagy can be caused by four parallel mechanisms, which are compatible with the data observed. First, LLPS of PRM-containing WNK1 and its multiple hypophosphorylations may trigger its activity loss. Second, abnormal interactions of the PRM and SH3 domain in hyperphosphorylated TP53BP2–ASPP2 may modify its autophagy initiation role (199, 200). As third and perhaps critical ALS-associated mechanism, a partial deficiency of OPTN may be caused by its association with PRM-containing hyperphosphorylated TOM1 and hypophosphorylated TOM1L2 (Supplemental Table S1*K*) and its association with accumulated SH3-containing MYO6. Fourth and perhaps most importantly among ALS-associated mechanisms, the massive hyperphosphorylation of PRM-containing SQSTM1 may reflect the outstanding cellular efforts to promote this aggrephagy process. This compensatory mechanism may parallel its exceptionally rapid inducibility after oxidative stress by NaARS but contrasts with its restricted availability upon autophagy interference by BafA1 in SCA2 cell models. Given that ATXN2 was observed to bind *Sqstm1* mRNA directly and that SQSTM1 acts as the SAR that mediates the trafficking of phase-separated polyQ-expanded ATXN2 to MTOC-associated aggregates and to subsequent proteolytic degradation *via* autophagosomes–lysosomes, this pathway may contain key targets for neuroprotective therapy approaches.

Phosphosite Regulation of Protein Activity in Autophagy and Proteostasis

The phosphorylation changes reveal the primary switches where cellular compensation efforts occur. Their detailed analysis may guide researchers to the pathways where damage responses are impaired or insufficient. Such molecular events may be key targets for pharmacological efforts to prevent or postpone the clinical onset of motor deficits.

The strong hyperphosphorylation events in proteostasis factors may provide clues about regulatory mechanisms, which may become useful in the development of neuroprotective therapies. Certainly, it is important to consider in detail whether phosphorylation events such as pSer152-SQSTM1, pSer207/Ser224/Ser226-SQSTM1, pSer344/Ser351/Ser357/Ser363-SQSTM1, and pSer547-OPTN represent an ALS-specific phosphoprofile among the SAR of aggrephagy, and pSer267/Ser271-UBQLN2 represents an ALS-specific phosphoprofile of this misfolded protein delivery factor to proteasome and/or autophagy.

SQSTM1, with its fivefold increased abundance, is the primary interest for researchers into the aggrephagy mechanisms in SCA2 and ALS, given that its mutation can result in a neurodegenerative process with the phenotype of ALS type 3 (141). Its 107.6-fold hyperphosphorylation within the ZZ domain (as cargo binding sequence) at pSer152-SQSTM1 was previously attributed to TBK1 (201), a Ser/Thr kinase whose mutation causes ALS (202). In addition, three clusters of phosphosites were located within an intrinsically disordered region. First, three phosphosites between aa 207 and 226 (pSer207 under control of RNF166 as an autophagy regulator (203)) with on average 36.7-fold increases were clustered in the vicinity of the TBS motif, where TRAF6 binding modulates the neurotrophin signaling cascades (204). Second, three phosphosites between aa 334 and 344 with on average 42.7-fold increases were clustered in the vicinity of the LIR motif, where LC3 binding determines the association of SQSTM1 with autophagosome membranes (204). Third, four phosphosites between amino acids 351 and 363 with an average 32.9-fold increases were clustered in the vicinity of the KIR motif, where KEAP1 binding modulates the NRF2-dependent transcription of detoxifying, cytoprotective, antioxidant, and inflammation-modulating factors (204). Thus, the SQSTM1 hyperphosphorylations may alter not only the association with autophagosomes but also with aggregate cargo and with cellular types of machinery for trophic signaling and stress responses. They are located in areas that explain the altered stress responses preferentially for nervous

tissue and may constitute an ALS-specific pattern within pathogenesis.

Despite its decreased abundance, OPTN showed a 2.7-fold increase of pSer187 within the LIR domain, which regulates the binding to autophagosome membranes, and a 10.0-fold increase of pSer547 close to the ZF motif and within the binding area for the ER-to-Golgi vesicle traffic regulator RAB1A and for TAX1 in competition with TAX1BP1 (132, 133). As mentioned, OPTN mutations cause ALS type 12 (205). Furthermore, OPTN is regulated by the ALS-associated kinase TBK1 (206, 207).

The 10.7-fold increase of pSer313-TAX1BP1 is in the vicinity of the O-homodimerization motif (aa 320–340) (208) and between the coiled-coil CC1 domain (aa 154–307) and the CC2 domain (aa 349–476) that is responsible for self-oligomerization (209). So far, TAX1BP1 was not found to be associated with selective neurodegeneration phenotypes such as ALS or ataxia, but it is targeted by the ALS-associated kinase TBK1 and interacts with the TBK1-regulated putative ALS disease protein and neuroinflammation repressor TNIP1 (aka ABIN1). TNIP1 inhibits selective autophagy *via* competition with SARs, and TNIP1 abundance is controlled by autophagy (210–217). A 2.7-fold hyperphosphorylation at pSer279-TNIP1 implicates this factor in SCA2–ALS13 pathogenesis. Apparently, TAX1BP1 plays its main role in the amplification of the aggregation process and the maturation of autophagosomes.

NBR1 as the archetypal SAR in aggrephagy (218, 219) is not associated with ALS. It showed >2.5-fold increased abundance in the KIN spinal cord, appeared regulated in reciprocal relation to SQSTM1 in cultured cells, and its KIN spinal cord phosphoprofile showed increases in two areas. These hyperphosphorylations were 6.4-fold at pSer116 and 9.8-fold at pSer117 in proximity to the homomultimerization domain PB1 and 2.2-fold at pThr647 between the LIR1 and LIR2 domains responsible for autophagosome membrane binding (219). Thus, cargo–protein interactions were not modulated in contrast to SQSTM1 and OPTN.

Despite the physiological localization of ATXN2 with the rough endoplasmic reticulum (rER) (43) and its relocalization to stress granules after cell damage (58), no putative ribophagy or ER-phagy receptor (such as NUFIP1, FAM134B, RTN3L, SEC62, CCPG1, ATL3, TEX264, NIPSNAP1/2) appeared hyperphosphorylated. Only the hyperphosphorylation of UBQLN2, with its ability to access phase-separated RNP complexes and to degrade rER proteins *via* the proteasome or *via* lysosomes (220), with an ALS phenotype upon mutation (221, 222), appeared to relate to the RNA-binding features of ATXN2 and to its preferential impact on motor neurons. UBQLN2 hyperphosphorylations at pSer271 (17.2-fold) and pSer267 (14.6-fold) were located in the middle of the four STI1 domains, where the association with molecular chaperones is regulated (223). Subsequent to chaperone interaction, UBQLN2 can either activate the ubiquitin–proteasome pathway of proteolysis or promote autophagolysosome formation. Both hyperphosphorylations are closest to the second STI1 domain, where LLPS is modulated, and the relocalization to stress granules and RNP complexes is determined (224, 225), so that UBQLN2 can promote the disposal of rER proteins (220). This preferential role for RNA-associated protein elimination may underlie the specific strong link between UBQLN2 mutations and the ALS phenotype (223, 224, 226).

The hyperphosphorylation of HSPB1 may also reflect cellular efforts to promote refolding and chaperone-mediated autophagy, particularly of the actin cytoskeleton and RNA granules (227–229).

WDFY3 abundance was increased almost threefold in the KIN spinal cord, so the 3.2-fold elevated presence of pThr818 may only reflect the accumulation of this activator of selective aggrephagy that cooperates with SQSTM1, LC3-II, and ATG proteins (230–232). This phosphosite lies within an Armadillo-like multihelical fold (residues 460–940) that is crucial in the yeast autophagy factor Vac8 for the association with disordered extended C termini of ATG proteins, the recruitment of cargo, and the link with membranes of the proteolytic vacuole (233).

The 8.7-fold increase of pSer216-CTSB is within the heavy chain area where several post-translational regulations occur, at aa 211 as part of a disulfide bond, at aa 220 where an N6-acetyl-lysine modification was observed (234), and at aa 240 where S-nitrosylation controls enzyme activity (235). CTSB can be secreted (236), but in lysosomes, it also serves as an apical regulator that is in control of overall lysosomal dynamics and autophagy (237). Again, CTSB has no association with ALS; it seems to be a nonspecific factor in autophagolysosomal pathology.

In contrast, BNIP3 acts in mitophagy, exhibits a widespread nonselective phosphorylation increase of a mild degree, and is also not associated with ALS. BNIP3 abundance was increased >3-fold, so the elevated amounts of phosphopeptides (2.2-fold at pSer48, 2.3-fold at pSer79, and 2.4-fold at pSer85, pThr86, and pSer88) may only be a secondary phenomenon. Altered mitophagy *via* BNIP3 adaptation to polyQ expansion may serve to explain the induction of *Pink1* mRNA as a kinase responsible for mitochondrial degradation in the blood of SCA2 patients (238).

Overall, the cellular efforts to optimize autophagy for the degradation of polyQ-expanded ATXN2 aggregates involve phosphorylations and adjusted abundance of several proteostasis factors, namely 1) in the cargo recognition domain of SQSTM1, 2) in the LIR motifs of SQSTM1 and OPTN, 3) in the homomultimerization domains of TAX1BP1 and NBR1, 4) regarding chaperone–proteasome roles *via* UBQLN2 and HSP1B, and 5) regarding lysosome availability *via* WDFY3 and CTSB. Elevated mitophagy may be a side effect of polyQ–ATXN2 aggregate degradation.

Mild Phosphorylation Reductions in ATXN2 C-Term, ATXN2L, RNPs, and PPIA

The physiological functions of ATXN2 and ATXN2L are adjusted with minor phosphorylation changes, and also other RNPs do not appear altered among the prominent phosphosites. The reduced appearance of phosphosites in ATXN2 from pSer319 at the LSm domain until the C-terminus upon polyQ expansion is probably a consequence of its impaired transcription and translation. Most of these hypophosphorylated sites are clustered within the IDR2 of ATXN2 (Fig. 1*B*), where microtubule binding is determined, and where a mild influence on mRNA and RNP binding was documented (49, 52, 239). In view of the combination of a C-terminal partial loss-of-function *versus* an N-terminal neurotoxic gain of function, it was interesting to examine the regulation of its paralog ATXN2L. Previous studies in ATXN2L-mutant cells had not observed an adaptation of ATXN2 levels and *vice versa* (37), so the functional relationship between the two gene copies had remained unclear. The RNP ATXN2L has higher levels than its paralog ATXN2 and exerts an essential role in embryonic development (37). As a novel insight, a mild hyperphosphorylation (4.1-fold) of presumably compensatory nature occurred in ATXN2L at pSer333, within the IDR2 very close to the LSm-AD region (aa 262–331) (Supplemental Fig. S1), where binding to RNA helicases like DDX6 is thought to impact the processing of mRNAs and the silencing of transcripts (42, 58–60). This ATXN2L pSer333 change is known to be controlled by protein kinase D1 (PRKD1), as documented in the Internet database at www.phosphositeplus.org (last accessed on February 28, 2024). This finding provides insight into the signaling mechanisms that govern ATXN2L physiology. It was previously established that ATXN2 *via* its PRMs modulates the uptake of trophic factor receptors such as epidermal growth factor receptor, *via* binding to SH3 motifs in endosome trafficking proteins such as SRC and GRB2 (65, 67) and that ATXN2 can localize to the trans-Golgi network (240). Therefore, it is very noteworthy that PRKD1 also acts in the Golgi apparatus, converting transient diacylglycerol signals to control Golgi integrity, establishing trafficking polarity, and delivering membrane proteins to neuronal dendrites for the maintenance of arborizations, in particular in cerebellar Purkinje cells (241–245). PRKD1 also stabilizes actin in dendritic spines with consequences for synaptic plasticity and long-term memory (246), modulates the endocytosis of α-amino-3-hydroxy-5-methyl-4-isoxazolepropionic acid receptors in glutamatergic postsynapses (247), and confers neuroprotection against excitotoxicity (248–251). Mutant PRKD1 leads to an age-dependent decline of locomotion rate in *Caenorhabditis elegans* nematode worms (252). Beyond its well-documented roles in neurons, PRKD1 also acts in glial cells to control nutrient uptake *via* micropinocytosis as well as protein aggregate uptake *via* phagocytosis (253). Thus, the impact of deficient PRKD1 function has a close resemblance to the features of SCA2 and acts on similar subcellular compartments as ATXN2–ATXN2L.

It is noteworthy that our MS data in Q100-KIN mouse spinal cord did not replicate the increase of pTDP-43 upon ATXN2 intermediate polyQ expansions, which was reported based on quantitative immunoblots in postmortem spinal cords from ALS cases (254). Contrasting with RNPs, their associated folding modulator PPIA showed an accumulation in immunoblots from the KIN spinal cord possibly because of altered TDP-43 association, and accompanied by a relevant 4.1-fold increase of pSer159-PPIA. These observations suggest that cellular compensatory efforts against ALS pathogenesis are targeting this molecular switch. The location of this phosphosite in the PPIA C-terminal region is close to several N6-acetyl-lysine modifications at aa 125, where interaction with TDP-43 is modulated (255).

Are Pathogenic or Compensatory Phosphorylation Changes Suitable Targets for Intervention?

Although the particularly massive hyperphosphorylations are at the center of our interest, and may constitute targets of novel neuroprotective approaches, a cautionary comment has to be made. Similarly striking findings were previously observed in protein aggregation–driven neurodegenerative disorders, as in the disease protein Tau (*e.g.*, at its 233Pro-Lys-pSer-Pro motif) for Alzheimer's disease and FTD (256–258), and in the disease protein TDP-43 (at its C-terminal 404pSer-pSer-Met-Asp-Ser-Lys-pSer-pSer motif) for ALS and FTD (259, 260). However, it has been proven very difficult to distinguish between protective *versus* toxic phosphorylation events; even for the hyperphosphorylation of TDP-43, the subsequent experiments have claimed either a compensatory role to prevent pathogenic TDP-43 isoforms from aggregation (260–263), or a contrary pathogenic role (264, 265), or a role according to residue and context (266, 267). Clearly, hyperphosphorylation can provide a crucial clue to define, which proteins and polypeptides are most affected by aggregation, and where LLPS would lead to massive conformational changes. However, the skillful adaptation of site-specific phosphorylation dosage to progressive stages of disease is currently difficult.

Study Limitations

In reviewing changes observed between conditions, it is important to note that some modified peptides were observed only once across all LC–MS/MS runs. Although the data have been filtered at both the peptide and protein levels, changes for peptides identified a single time should be interpreted with caution. These peptides are marked in Supplemental Table S1 with a "1" in the "Count in Details" column of the Summary tab. It was ensured that none of the dysregulations that are mentioned in the *Discussion* section refers to such data. Of course, the biggest study limitation consists in the fact that phosphoantibodies are not available for the great

majority of the MS findings here, so a validation of phosphorylation changes with a second technique was impossible.

Conclusion

Novel insights regarding the ATXN2 interactome and the adjustment of cell phosphosignals upon Q100-ATXN2 expansion indicate a prominent role of abnormal PRM–SH3 interactions that affect endocytosis/autophagy, actomyosin cytoskeleton, and synaptic pathways directly. Although the validation of proteome-wide phosphorylation patterns by independent methodology is currently impossible, the similarity of our findings to well-established pathomechanisms in HD provides high credibility to our observations. The pathways mentioned previously are probably crucial for efficacious preventive therapy, so future efforts to knock down *ATXN2* should target exons 1-3, particularly the N-terminal PRMs.

DATA AVAILABILITY

The phosphoproteome data are being deposited in the publically available repository PRIDE and can be accessed with the dataset identifier PXD062823.

INSTITUTIONAL REVIEW BOARD STATEMENT

The study was conducted in accordance with the Declaration of Helsinki. The analysis of human fibroblasts was approved by the Institutional Review Board (or Ethics Committee) of the Goethe University Frankfurt Medical School (protocol code 147/7, approved on June 26, 2007). The animal study protocol was approved by the Regierungspräsidium Darmstadt (protocol code V54-19c18-FK/1083, approved on March 27, 2017).

INFORMED CONSENT

Written informed consent was obtained from all subjects involved in the study.

Supplemental Data—This article contains supplemental data.

Acknowledgments—For technical assistance, we are grateful to Gabriele Köpf in the laboratory and to the staff of the ZFE animal facility at the Goethe University in Frankfurt. For technical help and informatics advice regarding the phosphoproteome, we thank the team at Cell Signaling Technologies, Inc, Danvers, MA, USA. We also thank the Center for Functional Proteomics at the Goethe University in Frankfurt for MS support.

Author Contributions—S. G. and G. A. conceptualization; J. C.- P., M. P. S., K. A., and S. G. methodology; A. R. K. and J. K. software; L.- E. A.- M., A. R. K., N.- E. S., J. C.- P., J. K., and S. G. validation; M. P. S., K. A., and G. A. formal analysis; L.- E. A.- M., A. R. K., L.- M. B., M. PS., and K. A. investigation; N.- E. S., J. C.- P., and S. G. resources; M. P. S. and G. A. data curation; L.- E. A.- M., A. R. K., J. K., and G. A. writing–original draft; L.- E. A.- M., A. R. K., N.- E. S., M. P. S., J. K., and S. G. writing–review & editing; L.- E. A.- M., A. R. K., J. C.- P., J. K., and G. A. visualization; M. P. S. supervision; S. G. and G. A. project administration; G. A. funding acquisition.

Funding and Additional Information—This research was funded by the Deutsche Forschungsgemeinschaft (grants AU96/11-1, 11-3, 16-1, and 21-1; to G.A.).

Conflict of Interest—The authors declare no competing interests. The funders had no role in the design of the study; in the collection, analyses, or interpretation of data; in the writing of the article; or in the decision to publish the results.

Abbreviations—The abbreviations used are: ALS, amyotrophic lateral sclerosis; ASO, antisense oligonucleotide; ATXN2, ataxin-2; ATXN2L, ataxin-2-like; BafA1, bafilomycin A1; CAG, cytosine–adenine–guanine; CIN85, Cbl-interacting protein of 85kDa; ER, endoplasmic reticulum; FDR, false discovery rate; FTD, frontotemporal dementia; HD, Huntington's disease; IDR, intrinsically disordered region; IMAC, immobilized metal affinity chromatography; KIN, knockin; LIR, LC3-interacting region; LLPS, liquid–liquid phase separation; LSm, like-Sm domain in cytoplasmic protein; LSm-AD, LSm-associated domain; MEF, mouse embryonic fibroblast; MS, mass spectrometry; MTOC, microtubule-organizing center; mTORC1, mechanistic target of rapamycin complex 1; MYO6, unconventional myosin VI; NaARS, sodium arsenite; OPTN, optineurin; PABPC1, poly(A)-binding protein 1; PAM2, poly(A)-binding protein–associated motif 2; PolyQ, polyglutamine; PRKD1, protein kinase D1; PRM, proline-rich motif; qPCR, quantitative PCR; rER, rough endoplasmic reticulum; RNP, ribonucleoprotein; RPL21, ribosomal protein large subunit component 21; RTK, receptor tyrosine kinase; SAR, selective autophagy receptor; SCA2, spinocerebellar ataxia type 2; SH3, SRC-homology domain type 3; SPARCL1, secreted protein acidic and cysteine rich-like 1; STRING, search tool for the retrieval of interacting genes; TDP-43/TARDBP, TAR DNA-binding protein 43; TNIP1/ABIN1, TNFAIP3 interacting protein 1; WNK1, protein kinase with no lysine 1.

Received April 21, 2025, and in revised form, September 14, 2025
Published, MCPRO Papers in Press, September 22, 2025, https://doi.org/10.1016/j.mcpro.2025.101072

REFERENCES

1. Pulst, S. M., Nechiporuk, A., Nechiporuk, T., Gispert, S., Chen, X. N., Lopes-Cendes, I., *et al*. (1996) Moderate expansion of a normally biallelic trinucleotide repeat in spinocerebellar ataxia type 2. *Nat. Genet.* **14**, 269–276
2. Sanpei, K., Takano, H., Igarashi, S., Sato, T., Oyake, M., Sasaki, H., *et al*. (1996) Identification of the spinocerebellar ataxia type 2 gene using a

direct identification of repeat expansion and cloning technique, DIRECT. *Nat. Genet.* **14**, 277–284
3. Imbert, G., Saudou, F., Yvert, G., Devys, D., Trottier, Y., Garnier, J. M., *et al*. (1996) Cloning of the gene for spinocerebellar ataxia 2 reveals a locus with high sensitivity to expanded CAG/glutamine repeats. *Nat. Genet.* **14**, 285–291
4. Orozco Diaz, G., Nodarse Fleites, A., Cordovés Sagaz, R., and Auburger, G. (1990) Autosomal dominant cerebellar ataxia: clinical analysis of 263 patients from a homogeneous population in Holguin, Cuba. *Neurology* **40**, 1369–1375
5. Auburger, G. W. (2012) Spinocerebellar ataxia type 2. *Handb Clin. Neurol.* **103**, 423–436
6. Almaguer-Mederos, L. E., Aguilera Rodríguez, R., González Zaldivar, Y., Almaguer Gotay, D., Cuello Almarales, D., Laffita Mesa, J., *et al*. (2013) Estimation of survival in spinocerebellar ataxia type 2 Cuban patients. *Clin. Genet.* **83**, 293–294
7. Rub, U., Schöls, L., Paulson, H., Auburger, G., Kermer, P., Jen, J. C., *et al*. (2013) Clinical features, neurogenetics and neuropathology of the polyglutamine spinocerebellar ataxias type 1, 2, 3, 6 and 7. *Prog. Neurobiol.* **104**, 38–66
8. Almaguer-Mederos, L. E., Pérez-Ávila, I., Aguilera-Rodríguez, R., Velázquez-Garcés, M., Almaguer-Gotay, D., Hechavarría-Pupo, R., *et al*. (2021) Body mass index is significantly associated with disease severity in spinocerebellar ataxia type 2 patients. *Mov. Disord.* **36**, 1372–1380
9. Elden, A. C., Kim, H. J., Hart, M. P., Chen-Plotkin, A. S., Johnson, B. S., Fang, X., *et al*. (2010) Ataxin-2 intermediate-length polyglutamine expansions are associated with increased risk for ALS. *Nature* **466**, 1069–1075
10. Lee, T., Li, Y. R., Ingre, C., Weber, M., Grehl, T., Gredal, O., *et al*. (2011) Ataxin-2 intermediate-length polyglutamine expansions in European ALS patients. *Hum. Mol. Genet.* **20**, 1697–1700
11. Gispert, S., Kurz, A., Waibel, S., Bauer, P., Liepelt, I., Geisen, C., *et al*. (2012) The modulation of Amyotrophic lateral sclerosis risk by ataxin-2 intermediate polyglutamine expansions is a specific effect. *Neurobiol. Dis.* **45**, 356–361
12. Lahut, S., Ömür, Ö., Uyan, Ö., Ağım, Z. S., Özoğuz, A., Parman, Y., *et al*. (2012) ATXN2 and its neighbouring gene SH2B3 are associated with increased ALS risk in the Turkish population. *PLoS One* **7**, e42956
13. Sproviero, W., Shatunov, A., Stahl, D., Shoai, M., van Rheenen, W., Jones, A. R., *et al*. (2017) ATXN2 trinucleotide repeat length correlates with risk of ALS. *Neurobiol. Aging* **51**, 178.e1–178.e9
14. Chio, A., Moglia, C., Canosa, A., Manera, U., Grassano, M., Vasta, R., *et al*. (2023) Association of copresence of pathogenic variants related to amyotrophic lateral sclerosis and prognosis. *Neurology* **101**, e83–e93
15. Fournier, C., Anquetil, V., Camuzat, A., Stirati-Buron, S., Sazdovitch, V., Molina-Porcel, L., *et al*. (2018) Interrupted CAG expansions in ATXN2 gene expand the genetic spectrum of frontotemporal dementias. *Acta Neuropathol. Commun.* **6**, 41
16. Rubino, E., Mancini, C., Boschi, S., Ferrero, P., Ferrone, M., Bianca, S., *et al*. (2019) ATXN2 intermediate repeat expansions influence the clinical phenotype in frontotemporal dementia. *Neurobiol. Aging* **73**, 231.e7–231.e9
17. Glass, J. D., Dewan, R., Ding, J., Gibbs, J. R., Dalgard, C., Keagle, P. J., *et al*. (2022) ATXN2 intermediate expansions in amyotrophic lateral sclerosis. *Brain* **145**, 2671–2676
18. Ross, O. A., Rutherford, N. J., Baker, M., Soto-Ortolaza, A. I., Carrasquillo, M. M., DeJesus-Hernandez, M., *et al*. (2011) Ataxin-2 repeat-length variation and neurodegeneration. *Hum. Mol. Genet.* **20**, 3207–3212
19. Kim, Y. E., Jeon, B., Farrer, M. J., Scott, E., Guella, I., Park, S. S., *et al*. (2017) SCA2 family presenting as typical Parkinson's disease: 34 year follow up. *Parkinsonism Relat. Disord.* **40**, 69–72
20. Kwong, L. K., Neumann, M., Sampathu, D. M., Lee, V. M. Y., and Trojanowski, J. Q. (2007) TDP-43 proteinopathy: the neuropathology underlying major forms of sporadic and familial frontotemporal lobar degeneration and motor neuron disease. *Acta Neuropathol.* **114**, 63–70
21. Liao, Y. Z., Ma, J., and Dou, J. Z. (2022) The role of TDP-43 in neurodegenerative disease. *Mol. Neurobiol.* **59**, 4223–4241
22. Highley, J. R., Lorente Pons, A., Cooper-Knock, J., Wharton, S. B., Ince, P. G., Shaw, P. J., *et al*. (2016) Motor neurone disease/amyotrophic lateral sclerosis associated with intermediate-length CAG repeat expansions in Ataxin-2 does not have 1C2-positive polyglutamine inclusions. *Neuropathol. Appl. Neurobiol.* **42**, 377–389
23. Watanabe, R., Higashi, S., Nonaka, T., Kawakami, I., Oshima, K., Niizato, K., *et al*. (2020) Intracellular dynamics of Ataxin-2 in the human brains with normal and frontotemporal lobar degeneration with TDP-43 inclusions. *Acta Neuropathol. Commun.* **8**, 176
24. Koyano, S., Yagishita, S., Tada, M., Doi, H., Uchihara, T., and Tanaka, F. (2022) Parallel appearance of polyglutamine and transactivation-responsive DNA-binding protein 43 and their complementary subcellular localization in brains of patients with spinocerebellar ataxia type 2. *J. Neuropathol. Exp. Neurol.* **81**, 535–544
25. [preprint] Wijegunawardana, D., Vishal, S. S., Venkatesh, N., and Gopal, P. P. (2023) Ataxin-2 polyglutamine expansions aberrantly sequester TDP-43, drive ribonucleoprotein condensate transport dysfunction and suppress local translation. *bioRxiv*. https://doi.org/10.1101/2023.01.30.526372
26. Becker, L. A., Huang, B., Bieri, G., Ma, R., Knowles, D. A., Jafar-Nejad, P., *et al*. (2017) Therapeutic reduction of ataxin-2 extends lifespan and reduces pathology in TDP-43 mice. *Nature* **544**, 367–371
27. Zeballos, C. M., Moore, H. J., Smith, T. J., Powell, J. E., Ahsan, N. S., Zhang, S., and Gaj, T. (2023) Mitigating a TDP-43 proteinopathy by targeting ataxin-2 using RNA-targeting CRISPR effector proteins. *Nat. Commun.* **14**, 6492
28. Wijegunawardana, D., Nayak, A., Vishal, S. S., Venkatesh, N., and Gopal, P. P. (2025) Ataxin-2 polyglutamine expansions aberrantly sequester TDP-43 ribonucleoprotein condensates disrupting mRNA transport and local translation in neurons. *Dev. Cell* **60**, 253–269
29. Scoles, D. R., Meera, P., Schneider, M. D., Paul, S., Dansithong, W., Figueroa, K. P., *et al*. (2017) Antisense oligonucleotide therapy for spinocerebellar ataxia type 2. *Nature* **544**, 362–366
30. Scoles, D. R., Gandelman, M., Paul, S., Dexheimer, T., Dansithong, W., Figueroa, K. P., *et al*. (2022) A quantitative high-throughput screen identifies compounds that lower expression of the SCA2-and ALS-associated gene ATXN2. *J. Biol. Chem.* **298**, 102228
31. Afonso, I. T., Lima, P., Conceição, A., Matos, C. A., and Nóbrega, C. (2022) Mutant ataxin-2 expression in aged animals aggravates neuropathological features associated with spinocerebellar ataxia type 2. *Int. J. Mol. Sci.* **23**, 11896
32. Marcelo, A., Afonso, I. T., Afonso-Reis, R., Brito, D. V. C., Costa, R. G., Rosa, A., *et al*. (2021) Autophagy in Spinocerebellar ataxia type 2, a dysregulated pathway, and a target for therapy. *Cell Death Dis.* **12**, 1117
33. Wardman, J. H., Henriksen, E. E., Marthaler, A. G., Nielsen, J. E., and Nielsen, T. T. (2020) Enhancement of autophagy and solubilization of ataxin-2 alleviate apoptosis in spinocerebellar ataxia type 2 patient cells. *Cerebellum* **19**, 165–181
34. Lastres-Becker, I., Brodesser, S., Lütjohann, D., Azizov, M., Buchmann, J., Hintermann, E., *et al*. (2008) Insulin receptor and lipid metabolism pathology in ataxin-2 knock-out mice. *Hum. Mol. Genet.* **17**, 1465–1481
35. Meierhofer, D., Halbach, M., Şen, N. E., Gispert, S., and Auburger, G. (2016) Ataxin-2 (Atxn2)-Knock-Out mice show branched chain amino acids and fatty acids pathway alterations. *Mol. Cell Proteomics* **15**, 1728–1739
36. Seidel, G., Meierhofer, D., Şen, N. E., Guenther, A., Krobitsch, S., and Auburger, G. (2017) Quantitative global proteomics of yeast PBP1 deletion mutants and their stress responses identifies glucose metabolism, mitochondrial, and stress granule changes. *J. Proteome Res.* **16**, 504–515
37. Key, J., Harter, P. N., Sen, N. E., Gradhand, E., Auburger, G., and Gispert, S. (2020) Mid-gestation lethality of Atxn2l-ablated mice. *Int. J. Mol. Sci.* **21**, 5124
38. Jimenez-Lopez, D., and Guzman, P. (2014) Insights into the evolution and domain structure of Ataxin-2 proteins across eukaryotes. *BMC Res. Notes* **7**, 453
39. Mangus, D. A., Amrani, N., and Jacobson, A. (1998) Pbp1p, a factor interacting with Saccharomyces cerevisiae poly(A)-binding protein, regulates polyadenylation. *Mol. Cell Biol.* **18**, 7383–7396
40. Kozlov, G., Trempe, J. F., Khaleghpour, K., Kahvejian, A., Ekiel, I., and Gehring, K. (2001) Structure and function of the C-terminal PABC

domain of human poly(A)-binding protein. *Proc. Natl. Acad. Sci. U. S. A.* **98**, 4409–4413
41. Ciosk, R., DePalma, M., and Priess, J. R. (2004) ATX-2, the C. elegans ortholog of ataxin 2, functions in translational regulation in the germline. *Development* **131**, 4831–4841
42. Satterfield, T. F., and Pallanck, L. J. (2006) Ataxin-2 and its Drosophila homolog, ATX2, physically assemble with polyribosomes. *Hum. Mol. Genet.* **15**, 2523–2532
43. van de Loo, S., Eich, F., Nonis, D., Auburger, G., and Nowock, J. (2009) Ataxin-2 associates with rough endoplasmic reticulum. *Exp. Neurol.* **215**, 110–118
44. Damrath, E., Heck, M. V., Gispert, S., Azizov, M., Nowock, J., Seifried, C., *et al*. (2012) ATXN2-CAG42 sequesters PABPC1 into insolubility and induces FBXW8 in cerebellum of old ataxic knock-in mice. *PLoS Genet.* **8**, e1002920
45. Lim, C., and Allada, R. (2013) ATAXIN-2 activates PERIOD translation to sustain circadian rhythms in Drosophila. *Science* **340**, 875–879
46. Zhang, Y., Ling, J., Yuan, C., Dubruille, R., and Emery, P. (2013) A role for Drosophila ATX2 in activation of PER translation and circadian behavior. *Science* **340**, 879–882
47. Fittschen, M., Lastres-Becker, I., Halbach, M. V., Damrath, E., Gispert, S., Azizov, M., *et al*. (2015) Genetic ablation of ataxin-2 increases several global translation factors in their transcript abundance but decreases translation rate. *Neurogenetics* **16**, 181–192
48. Lastres-Becker, I., Nonis, D., Eich, F., Klinkenberg, M., Gorospe, M., Kötter, P., *et al*. (2016) Mammalian ataxin-2 modulates translation control at the pre-initiation complex via PI3K/mTOR and is induced by starvation. *Biochim. Biophys. Acta* **1862**, 1558–1569
49. Bakthavachalu, B., Huelsmeier, J., Sudhakaran, I. P., Hillebrand, J., Singh, A., Petrauskas, A., *et al*. (2018) RNP-granule assembly via ataxin-2 disordered domains is required for long-term memory and neurodegeneration. *Neuron* **98**, 754–766.e4
50. Inagaki, H., Hosoda, N., Tsuiji, H., and Hoshino, S. I. (2020) Direct evidence that Ataxin-2 is a translational activator mediating cytoplasmic polyadenylation. *J. Biol. Chem.* **295**, 15810–15825
51. Nadimpalli, H. P., Guitart, T., Coll, O., and Gebauer, F. (2022) Ataxin-2, Twenty-four, and Dicer-2 are components of a noncanonical cytoplasmic polyadenylation complex. *Life Sci. Alliance* **5**, e202201417
52. Boeynaems, S., Dorone, Y., Zhuang, Y., Shabardina, V., Huang, G., Marian, A., *et al*. (2023) Poly(A)-binding protein is an ataxin-2 chaperone that regulates biomolecular condensates. *Mol. Cell* **83**, 2020–2034.e6
53. Zhuang, Y., Li, Z., Xiong, S., Sun, C., Li, B., Wu, S. A., *et al*. (2023) Circadian clocks are modulated by compartmentalized oscillating translation. *Cell* **186**, 3245–3260.e23
54. Albrecht, M., and Lengauer, T. (2004) Novel Sm-like proteins with long C-terminal tails and associated methyltransferases. *FEBS Lett.* **569**, 18–26
55. Albrecht, M., Golatta, M., Wüllner, U., and Lengauer, T. (2004) Structural and functional analysis of ataxin-2 and ataxin-3. *Eur. J. Biochem.* **271**, 3155–3170
56. Lekontseva, N. V., Stolboushkina, E. A., and Nikulin, A. D. (2021) Diversity of LSM family proteins: similarities and differences. *Biochemistry (Mosc)* **86**(Suppl 1), S38–S49
57. Yokoshi, M., Li, Q., Yamamoto, M., Okada, H., Suzuki, Y., and Kawahara, Y. (2014) Direct binding of Ataxin-2 to distinct elements in 3' UTRs promotes mRNA stability and protein expression. *Mol. Cell* **55**, 186–198
58. Nonhoff, U., Ralser, M., Welzel, F., Piccini, I., Balzereit, D., Yaspo, M. L., *et al*. (2007) Ataxin-2 interacts with the DEAD/H-box RNA helicase DDX6 and interferes with P-bodies and stress granules. *Mol. Biol. Cell* **18**, 1385–1396
59. Lee, J., Yoo, E., Lee, H., Park, K., Hur, J. H., and Lim, C. (2017) LSM12 and ME31B/DDX6 define distinct modes of posttranscriptional regulation by ATAXIN-2 protein complex in Drosophila circadian pacemaker neurons. *Mol. Cell* **66**, 129–140.e7
60. Inagaki, H., Hosoda, N., and Hoshino, S. I. (2021) DDX6 is a positive regulator of Ataxin-2/PAPD4 cytoplasmic polyadenylation machinery. *Biochem. Biophys. Res. Commun.* **553**, 9–16
61. Ralser, M., Albrecht, M., Nonhoff, U., Lengauer, T., Lehrach, H., and Krobitsch, S. (2005) An integrative approach to gain insights into the cellular function of human ataxin-2. *J. Mol. Biol.* **346**, 203–214
62. Swisher, K. D., and Parker, R. (2010) Localization to, and effects of Pbp1, Pbp4, Lsm12, Dhh1, and Pab1 on stress granules in Saccharomyces cerevisiae. *PLoS One* **5**, e10006
63. Kaehler, C., Isensee, J., Nonhoff, U., Terrey, M., Hucho, T., Lehrach, H., and Krobitsch, S. (2012) Ataxin-2-like is a regulator of stress granules and processing bodies. *PLoS One* **7**, e50134
64. Wang, J. Y., Liu, Y. J., Zhang, X. L., Liu, Y. H., Jiang, L. L., and Hu, H. Y. (2024) PolyQ-expanded ataxin-2 aggregation impairs cellular processing-body homeostasis via sequestering the RNA helicase DDX6. *J. Biol. Chem.* **300**, 107413
65. Nonis, D., Schmidt, M. H. H., van de Loo, S., Eich, F., Dikic, I., Nowock, J., and Auburger, G. (2008) Ataxin-2 associates with the endocytosis complex and affects EGF receptor trafficking. *Cell Signal.* **20**, 1725–1739
66. Ariumi, Y., Kuroki, M., Kushima, Y., Osugi, K., Hijikata, M., Maki, M., *et al*. (2011) Hepatitis C virus hijacks P-body and stress granule components around lipid droplets. *J. Virol.* **85**, 6882–6892
67. Drost, J., Nonis, D., Eich, F., Leske, O., Damrath, E., Brunt, E. R., *et al*. (2013) Ataxin-2 modulates the levels of Grb2 and SRC but not ras signaling. *J. Mol. Neurosci.* **51**, 68–81
68. Auburger, G., Sen, N. E., Meierhofer, D., Başak, A. N., and Gitler, A. D. (2017) Efficient prevention of neurodegenerative diseases by depletion of starvation response factor ataxin-2. *Trends Neurosci.* **40**, 507–516
69. Bar, D. Z., Charar, C., Dorfman, J., Yadid, T., Tafforeau, L., Lafontaine, D. L. J., and Gruenbaum, Y. (2016) Cell size and fat content of dietary-restricted Caenorhabditis elegans are regulated by ATX-2, an mTOR repressor. *Proc. Natl. Acad. Sci. U. S. A.* **113**, E4620–E4629
70. Kato, M., Yang, Y. S., Sutter, B. M., Wang, Y., McKnight, S. L., and Tu, B. P. (2019) Redox state controls phase separation of the yeast ataxin-2 protein via reversible oxidation of its methionine-rich low-complexity domain. *Cell* **177**, 711–721.e8
71. Yang, Y. S., Kato, M., Wu, X., Litsios, A., Sutter, B. M., Wang, Y., *et al*. (2019) Yeast ataxin-2 forms an intracellular condensate required for the inhibition of TORC1 signaling during respiratory growth. *Cell* **177**, 697–710.e17
72. DeMille, D., Badal, B. D., Evans, J. B., Mathis, A. D., Anderson, J. F., and Grose, J. H. (2015) PAS kinase is activated by direct SNF1-dependent phosphorylation and mediates inhibition of TORC1 through the phosphorylation and activation of Pbp1. *Mol. Biol. Cell* **26**, 569–582
73. Liu, Y. J., Wang, J. Y., Zhang, X. L., Jiang, L. L., and Hu, H. Y. (2024) Ataxin-2 sequesters Raptor into aggregates and impairs cellular mTORC1 signaling. *FEBS J.* **291**, 1795–1812
74. Prouteau, M., and Loewith, R. (2019) TOR signaling is going through a phase. *Cell Metab* **29**, 1019–1021
75. Satterfield, T. F., Jackson, S. M., and Pallanck, L. J. (2002) A Drosophila homolog of the polyglutamine disease gene SCA2 is a dosage-sensitive regulator of actin filament formation. *Genetics* **162**, 1687–1702
76. Sen, N. E., and Auburger, G. (2023) Modeling amyotrophic lateral sclerosis through Ataxin-2 pathology. In: Preedy, V. R., Martin, C. R., Patel, V. B., eds. *Handbook of Animal Models in Neurological Disorders*, Acadmic Press, Cambridge, MA: 95–106
77. Sen, N. E., Canet-Pons, J., Halbach, M. V., Arsovic, A., Pilatus, U., Chae, W. H., *et al*. (2019) Generation of an Atxn2-CAG100 knock-in mouse reveals N-acetylaspartate production deficit due to early Nat8l dysregulation. *Neurobiol. Dis.* **132**, 104559
78. Bux, J., Sen, N. E., Klink, I. M., Hauser, S., Synofzik, M., Schöls, L., *et al*. (2023) TR-FRET-Based immunoassay to measure ataxin-2 as a target engagement marker in spinocerebellar ataxia type 2. *Mol. Neurobiol.* **60**, 3553–3567
79. Arsovic, A., Halbach, M. V., Canet-Pons, J., Esen-Sehir, D., Döring, C., Freudenberg, F., *et al*. (2020) Mouse ataxin-2 expansion downregulates CamKII and other calcium signaling factors, impairing granule-purkinje neuron synaptic strength. *Int. J. Mol. Sci.* **21**, 6673
80. Sen, N. E., Arsovic, A., Meierhofer, D., Brodesser, S., Oberschmidt, C., Canet-Pons, J., *et al*. (2019) Human and mouse spino-cerebellar tissue, ataxin-2 expansion affects ceramide-sphingomyelin metabolism. *Int. J. Mol. Sci.* **20**, 5854
81. Canet-Pons, J., Sen, N. E., Arsović, A., Almaguer-Mederos, L. E., Halbach, M. V., Key, J., *et al*. (2021) Atxn2-CAG100-KnockIn mouse spinal cord shows progressive TDP43 pathology associated with cholesterol biosynthesis suppression. *Neurobiol. Dis.* **152**, 105289

82. Ragothaman, M., Sarangmath, N., Chaudhary, S., Khare, V., Mittal, U., Sharma, S., *et al*. (2004) Complex phenotypes in an Indian family with homozygous SCA2 mutations. *Ann. Neurol.* **55**, 130–133
83. Hoche, F., Balikó, L., den Dunnen, W., Steinecker, K., Bartos, L., Sáfrány, E., *et al*. (2011) Spinocerebellar ataxia type 2 (SCA2): identification of early brain degeneration in one monozygous twin in the initial disease stage. *Cerebellum* **10**, 245–253
84. Tojima, M., Murakami, G., Hikawa, R., Yamakado, H., Yamashita, H., Takahashi, R., and Matsui, M. (2018) Homozygous 31 trinucleotide repeats in the SCA2 allele are pathogenic for cerebellar ataxia. *Neurol. Genet.* **4**, e283
85. Truett, G. E., Heeger, P., Mynatt, R. L., Truett, A. A., Walker, J. A., and Warman, M. L. (2000) Preparation of PCR-quality mouse genomic DNA with hot sodium hydroxide and tris (HotSHOT). *Biotechniques* **29**, 52–54
86. Stokes, M. P., Farnsworth, C. L., Gu, H., Jia, X., Worsfold, C. R., Yang, V., *et al*. (2015) Complementary PTM profiling of drug response in human gastric carcinoma by immunoaffinity and IMAC methods with total proteome analysis. *Proteomes* **3**, 160–183
87. Possemato, A. P., Paulo, J. A., Mulhern, D., Guo, A., Gygi, S. P., and Beausoleil, S. A. (2017) Multiplexed phosphoproteomic profiling using titanium dioxide and immunoaffinity enrichments reveals complementary phosphorylation events. *J. Proteome Res.* **16**, 1506–1514
88. Olsen, J. V., de Godoy, L. M. F., Li, G., Macek, B., Mortensen, P., Pesch, R., *et al*. (2005) Parts per million mass accuracy on an Orbitrap mass spectrometer via lock mass injection into a C-trap. *Mol. Cell Proteomics* **4**, 2010–2021
89. Eng, J. K., Jahan, T. A., and Hoopmann, M. R. (2013) Comet: an open-source MS/MS sequence database search tool. *Proteomics* **13**, 22–24
90. Huttlin, E. L., Jedrychowski, M. P., Elias, J. E., Goswami, T., Rad, R., Beausoleil, S. A., *et al*. (2010) A tissue-specific atlas of mouse protein phosphorylation and expression. *Cell* **143**, 1174–1189
91. Villen, J., Beausoleil, S. A., Gerber, S. A., and Gygi, S. P. (2007) Large-scale phosphorylation analysis of mouse liver. *Proc. Natl. Acad. Sci. U. S. A.* **104**, 1488–1493
92. Beausoleil, S. A., Villén, J., Gerber, S. A., Rush, J., and Gygi, S. P. (2006) A probability-based approach for high-throughput protein phosphorylation analysis and site localization. *Nat. Biotechnol.* **24**, 1285–1292
93. Hornbeck, P. V., Zhang, B., Murray, B., Kornhauser, J. M., Latham, V., and Skrzypek, E. (2015) PhosphoSitePlus, 2014: mutations, PTMs and recalibrations. *Nucleic Acids Res.* **43**, D512–D520
94. MacLean, B., Tomazela, D. M., Shulman, N., Chambers, M., Finney, G. L., Frewen, B., *et al*. (2010) Skyline: an open source document editor for creating and analyzing targeted proteomics experiments. *Bioinformatics* **26**, 966–968
95. Livak, K. J., and Schmittgen, T. D. (2001) Analysis of relative gene expression data using real-time quantitative PCR and the 2(-Delta Delta C(T)) Method. *Methods* **25**, 402–408
96. Szklarczyk, D., Gable, A. L., Lyon, D., Junge, A., Wyder, S., Huerta-Cepas, J., *et al*. (2019) STRING v11: protein-protein association networks with increased coverage, supporting functional discovery in genome-wide experimental datasets. *Nucleic Acids Res.* **47**, D607–d613
97. Brady, S. T., Mesnard-Hoaglin, N. A., Mays, S., Priego, M., Dziechciowska, J., Morris, S., *et al*. (2024) Toxic effects of mutant huntingtin in axons are mediated by its proline-rich domain. *Brain* **147**, 2098–2113
98. Crick, S. L., Ruff, K. M., Garai, K., Frieden, C., and Pappu, R. V. (2013) Unmasking the roles of N- and C-terminal flanking sequences from exon 1 of huntingtin as modulators of polyglutamine aggregation. *Proc. Natl. Acad. Sci. U. S. A.* **110**, 20075–20080
99. Dehay, B., and Bertolotti, A. (2006) Critical role of the proline-rich region in Huntingtin for aggregation and cytotoxicity in yeast. *J. Biol. Chem.* **281**, 35608–35615
100. Qin, Z. H., Wang, Y., Sapp, E., Cuiffo, B., Wanker, E., Hayden, M. R., *et al*. (2004) Huntingtin bodies sequester vesicle-associated proteins by a polyproline-dependent interaction. *J. Neurosci.* **24**, 269–281
101. Southwell, A. L., Khoshnan, A., Dunn, D. E., Bugg, C. W., Lo, D. C., and Patterson, P. H. (2008) Intrabodies binding the proline-rich domains of mutant huntingtin increase its turnover and reduce neurotoxicity. *J. Neurosci.* **28**, 9013–9020
102. Peskett, T. R., Rau, F., O'Driscoll, J., Patani, R., Lowe, A. R., and Saibil, H. R. (2018) A liquid to solid phase transition underlying pathological huntingtin Exon1 aggregation. *Mol. Cell* **70**, 588–601.e6
103. Uversky, V. N. (2017) The roles of intrinsic disorder-based liquid-liquid phase transitions in the "Dr. Jekyll-Mr. Hyde" behavior of proteins involved in amyotrophic lateral sclerosis and frontotemporal lobar degeneration. *Autophagy* **13**, 2115–2162
104. Gao, Y. G., Yan, X. Z., Song, A. X., Chang, Y. G., Gao, X. C., Jiang, N., *et al*. (2006) Structural insights into the specific binding of huntingtin proline-rich region with the SH3 and WW domains. *Structure* **14**, 1755–1765
105. Li, P., Banjade, S., Cheng, H. C., Kim, S., Chen, B., Guo, L., *et al*. (2012) Phase transitions in the assembly of multivalent signalling proteins. *Nature* **483**, 336–340
106. Amaya, J., Ryan, V. H., and Fawzi, N. L. (2018) The SH3 domain of Fyn kinase interacts with and induces liquid-liquid phase separation of the low-complexity domain of hnRNPA2. *J. Biol. Chem.* **293**, 19522–19531
107. Ghosh, A., Mazarakos, K., and Zhou, H. X. (2019) Three archetypical classes of macromolecular regulators of protein liquid-liquid phase separation. *Proc. Natl. Acad. Sci. U. S. A.* **116**, 19474–19483
108. Pankivskyi, S., Pastré, D., Steiner, E., Joshi, V., Rynditch, A., and Hamon, L. (2021) ITSN1 regulates SAM68 solubility through SH3 domain interactions with SAM68 proline-rich motifs. *Cell Mol. Life Sci.* **78**, 1745–1763
109. Martinez-Marmol, R., Small, C., Jiang, A., Palliyaguru, T., Wallis, T. P., Gormal, R. S., *et al*. (2023) Fyn nanoclustering requires switching to an open conformation and is enhanced by FTLD-Tau biomolecular condensates. *Mol. Psychiatry* **28**, 946–962
110. Lopez-Palacios, T. P., and Andersen, J. L. (2023) Kinase regulation by liquid-liquid phase separation. *Trends Cell Biol.* **33**, 649–666
111. Maier, J., Sieme, D., Wong, L. E., Dar, F., Wienands, J., Becker, S., and Griesinger, C. (2024) Quantitative description of the phase-separation behavior of the multivalent SLP65-CIN85 complex. *PNAS Nexus* **3**, pgae079
112. Kazemein Jasemi, N. S., Mehrabipour, M., Magdalena Estirado, E., Brunsveld, L., Dvorsky, R., and Ahmadian, M. R. (2024) Functional classification and interaction selectivity landscape of the human SH3 domain superfamily. *Cells* **13**, 195
113. Umemori, H., Sato, S., Yagi, T., Aizawa, S., and Yamamoto, T. (1994) Initial events of myelination involve Fyn tyrosine kinase signalling. *Nature* **367**, 572–576
114. Yamada, E., Bastie, C. C., Koga, H., Wang, Y., Cuervo, A. M., and Pessin, J. E. (2012) Mouse skeletal muscle fiber-type-specific macroautophagy and muscle wasting are regulated by a Fyn/STAT3/Vps34 signaling pathway. *Cell Rep.* **1**, 557–569
115. Yang, M., Liang, C., Swaminathan, K., Herrlinger, S., Lai, F., Shiekhattar, R., and Chen, J. F. (2016) A C9ORF72/SMCR8-containing complex regulates ULK1 and plays a dual role in autophagy. *Sci. Adv.* **2**, e1601167
116. Ciura, S., Sellier, C., Campanari, M. L., Charlet-Berguerand, N., and Kabashi, E. (2016) The most prevalent genetic cause of ALS-FTD, C9orf72 synergizes the toxicity of ATXN2 intermediate polyglutamine repeats through the autophagy pathway. *Autophagy* **12**, 1406–1408
117. Sellier, C., Campanari, M. L., Julie Corbier, C., Gaucherot, A., Kolb-Cheynel, I., Oulad-Abdelghani, M., *et al*. (2016) Loss of C9ORF72 impairs autophagy and synergizes with polyQ Ataxin-2 to induce motor neuron dysfunction and cell death. *EMBO J.* **35**, 1276–1297
118. Ke, P. Y. (2018) The multifaceted roles of autophagy in flavivirus-host interactions. *Int. J. Mol. Sci.* **19**, 3940
119. Conway, O., Akpinar, H. A., Rogov, V. V., and Kirkin, V. (2020) Selective autophagy receptors in neuronal health and disease. *J. Mol. Biol.* **432**, 2483–2509
120. Yang, C. S., Lee, J. S., Rodgers, M., Min, C. K., Lee, J. Y., Kim, H. J., *et al*. (2012) Autophagy protein Rubicon mediates phagocytic NADPH oxidase activation in response to microbial infection or TLR stimulation. *Cell Host Microbe* **11**, 264–276
121. Cipriano, A., Viviano, M., Feoli, A., Milite, C., Sarno, G., Castellano, S., and Sbardella, G. (2023) NADPH oxidases: from molecular mechanisms to current inhibitors. *J. Med. Chem.* **66**, 11632–11655

122. Gallolu Kankanamalage, S., Lee, A. Y., Wichaidit, C., Lorente-Rodriguez, A., Shah, A. M., Stippec, S., *et al*. (2016) Multistep regulation of autophagy by WNK1. *Proc. Natl. Acad. Sci. U. S. A.* **113**, 14342–14347
123. McCormick, J. A., and Ellison, D. H. (2011) The WNKs: atypical protein kinases with pleiotropic actions. *Physiol. Rev.* **91**, 177–219
124. Yamamoto, Y., Chino, H., Tsukamoto, S., Ode, K. L., Ueda, H. R., and Mizushima, N. (2021) NEK9 regulates primary cilia formation by acting as a selective autophagy adaptor for MYH9/myosin IIA. *Nat. Commun.* **12**, 3292
125. Cha-Molstad, H., Yu, J. E., Feng, Z., Lee, S. H., Kim, J. G., Yang, P., *et al*. (2017) p62/SQSTM1/Sequestosome-1 is an N-recognin of the N-end rule pathway which modulates autophagosome biogenesis. *Nat. Commun.* **8**, 102
126. Cha-Molstad, H., Lee, S. H., Kim, J. G., Sung, K. W., Hwang, J., Shim, S. M., *et al*. (2018) Regulation of autophagic proteolysis by the N-recognin SQSTM1/p62 of the N-end rule pathway. *Autophagy* **14**, 359–361
127. Ji, C. H., Kim, H. Y., Heo, A. J., Lee, S. H., Lee, M. J., Kim, S. B., *et al*. (2019) The N-degron pathway mediates ER-phagy. *Mol. Cell* **75**, 1058–1072.e9
128. Bonnet, L. V., Palandri, A., Flores-Martin, J. B., and Hallak, M. E. (2024) Arginyltransferase 1 modulates p62-driven autophagy via mTORC1/AMPk signaling. *Cell Commun. Signal.* **22**, 87
129. Varland, S., Vandekerckhove, J., and Drazic, A. (2019) Actin post-translational modifications: the cinderella of cytoskeletal control. *Trends Biochem. Sci.* **44**, 502–516
130. Chin, S. M., Hatano, T., Sivashanmugam, L., Suchenko, A., Kashina, A. S., Balasubramanian, M. K., and Jansen, S. (2022) N-terminal acetylation and arginylation of actin determines the architecture and assembly rate of linear and branched actin networks. *J. Biol. Chem.* **298**, 102518
131. Sahlender, D. A., Roberts, R. C., Arden, S. D., Spudich, G., Taylor, M. J., Luzio, J. P., *et al*. (2005) Optineurin links myosin VI to the Golgi complex and is involved in Golgi organization and exocytosis. *J. Cell Biol.* **169**, 285–295
132. Ryan, T. A., and Tumbarello, D. A. (2018) Optineurin: a coordinator of membrane-associated cargo trafficking and autophagy. *Front. Immunol.* **9**, 1024
133. Zhao, S., Chen, R., Gao, Y., Lu, Y., Bai, X., and Zhang, J. (2023) Fundamental roles of the optineurin gene in the molecular pathology of amyotrophic lateral sclerosis. *Front. Neurosci.* **17**, 1319706
134. Laplantine, E., Fontan, E., Chiaravalli, J., Lopez, T., Lakisic, G., Véron, M., *et al*. (2009) NEMO specifically recognizes K63-linked poly-ubiquitin chains through a new bipartite ubiquitin-binding domain. *EMBO J.* **28**, 2885–2895
135. Gan, K. J., and Sudhof, T. C. (2020) SPARCL1 promotes excitatory but not inhibitory synapse formation and function independent of neurexins and neuroligins. *J. Neurosci.* **40**, 8088–8102
136. Chen, S., Zou, Q., Chen, Y., Kuang, X., Wu, W., Guo, M., *et al*. (2020) Regulation of SPARC family proteins in disorders of the central nervous system. *Brain Res. Bull.* **163**, 178–189
137. Shimizu, H., Toyoshima, Y., Shiga, A., Yokoseki, A., Arakawa, K., Sekine, Y., *et al*. (2013) Sporadic ALS with compound heterozygous mutations in the SQSTM1 gene. *Acta Neuropathol.* **126**, 453–459
138. Soo, K. Y., Sultana, J., King, A. E., Atkinson, R., Warraich, S. T., Sundaramoorthy, V., *et al*. (2015) ALS-associated mutant FUS inhibits macroautophagy which is restored by overexpression of Rab1. *Cell Death Discov.* **1**, 15030
139. Madill, M., McDonagh, K., Ma, J., Vajda, A., McLoughlin, P., O'Brien, T., *et al*. (2017) Amyotrophic lateral sclerosis patient iPSC-derived astrocytes impair autophagy via non-cell autonomous mechanisms. *Mol. Brain* **10**, 22
140. Chitiprolu, M., Jagow, C., Tremblay, V., Bondy-Chorney, E., Paris, G., Savard, A., *et al*. (2018) A complex of C9ORF72 and p62 uses arginine methylation to eliminate stress granules by autophagy. *Nat. Commun.* **9**, 2794
141. Davidson, J. M., Chung, R. S., and Lee, A. (2022) The converging roles of sequestosome-1/p62 in the molecular pathways of amyotrophic lateral sclerosis (ALS) and frontotemporal dementia (FTD). *Neurobiol. Dis.* **166**, 105653
142. Millecamps, S., Boillée, S., Chabrol, E., Camu, W., Cazeneuve, C., Salachas, F., *et al*. (2011) Screening of OPTN in French familial amyotrophic lateral sclerosis. *Neurobiol. Aging* **32**, 557.e11–557.e13
143. van Blitterswijk, M., van Vught, P. W. J., van Es, M. A., Schelhaas, H. J., van der Kooi, A. J., de Visser, M., *et al*. (2012) Novel optineurin mutations in sporadic amyotrophic lateral sclerosis patients. *Neurobiol. Aging* **33**, 1016.e1–1016.e7
144. Kamada, M., Izumi, Y., Ayaki, T., Nakamura, M., Kagawa, S., Kudo, E., *et al*. (2014) Clinicopathologic features of autosomal recessive amyotrophic lateral sclerosis associated with optineurin mutation. *Neuropathology* **34**, 64–70
145. Pottier, C., Bieniek, K. F., Finch, N., van de Vorst, M., Baker, M., Perkersen, R., *et al*. (2015) Whole-genome sequencing reveals important role for TBK1 and OPTN mutations in frontotemporal lobar degeneration without motor neuron disease. *Acta Neuropathol.* **130**, 77–92
146. Gotkine, M., de Majo, M., Wong, C. H., Topp, S. D., Michaelson-Cohen, R., Epsztejn-Litman, S., *et al*. (2021) A recessive S174X mutation in Optineurin causes amyotrophic lateral sclerosis through a loss of function via allele-specific nonsense-mediated decay. *Neurobiol. Aging* **106**, 351.e1–351.e6
147. Prtenjaca, N., Rob, M., Alam, M. S., Markovinovic, A., Stuani, C., Buratti, E., and Munitic, I. (2022) Optineurin deficiency and insufficiency lead to higher microglial TDP-43 protein levels. *Int. J. Mol. Sci.* **23**, 6829
148. Li, C., Chen, Y., Chen, X., Wei, Q., Ou, R., Gu, X., *et al*. (2020) MicroRNA-183-5p is stress-inducible and protects neurons against cell death in amyotrophic lateral sclerosis. *J. Cell Mol. Med.* **24**, 8614–8622
149. Kim, H. C., Zhang, Y., King, P. H., and Lu, L. (2023) MicroRNA-183-5p regulates TAR DNA-binding protein 43 neurotoxicity via SQSTM1/p62 in amyotrophic lateral sclerosis. *J. Neurochem.* **164**, 643–657
150. Klionsky, D. J., Elazar, Z., Seglen, P. O., and Rubinsztein, D. C. (2008) Does bafilomycin A1 block the fusion of autophagosomes with lysosomes? *Autophagy* **4**, 849–850
151. McEwen, E., Kedersha, N., Song, B., Scheuner, D., Gilks, N., Han, A., *et al*. (2005) Heme-regulated inhibitor kinase-mediated phosphorylation of eukaryotic translation initiation factor 2 inhibits translation, induces stress granule formation, and mediates survival upon arsenite exposure. *J. Biol. Chem.* **280**, 16925–16933
152. Paul, S., Dansithong, W., Gandelman, M., Figueroa, K. P., Zu, T., Ranum, L. P. W., *et al*. (2023) Staufen impairs autophagy in neurodegeneration. *Ann. Neurol.* **93**, 398–416
153. Shi, J., Fung, G., Piesik, P., Zhang, J., and Luo, H. (2014) Dominant-negative function of the C-terminal fragments of NBR1 and SQSTM1 generated during enteroviral infection. *Cell Death Differ* **21**, 1432–1441
154. Sanchez-Martin, P., Sou, Y. S., Kageyama, S., Koike, M., Waguri, S., and Komatsu, M. (2020) NBR1-mediated p62-liquid droplets enhance the Keap1-Nrf2 system. *EMBO Rep.* **21**, e48902
155. Kozlov, G., Safaee, N., Rosenauer, A., and Gehring, K. (2010) Structural basis of binding of P-body-associated proteins GW182 and ataxin-2 by the MIle domain of poly(A)-binding protein. *J. Biol. Chem.* **285**, 13599–13606
156. Zhang, C., Gao, J., Li, M., Deng, Y., and Jiang, C. (2018) p38delta MAPK regulates aggresome biogenesis by phosphorylating SQSTM1 in response to proteasomal stress. *J. Cell Sci.* **131**, jcs216671
157. Mangiarini, L., Sathasivam, K., Seller, M., Cozens, B., Harper, A., Hetherington, C., *et al*. (1996) Exon 1 of the HD gene with an expanded CAG repeat is sufficient to cause a progressive neurological phenotype in transgenic mice. *Cell* **87**, 493–506
158. Sittler, A., Wälter, S., Wedemeyer, N., Hasenbank, R., Scherzinger, E., Eickhoff, H., *et al*. (1998) SH3GL3 associates with the Huntingtin exon 1 protein and promotes the formation of polygln-containing protein aggregates. *Mol. Cell* **2**, 427–436
159. Murphy, K. P., Carter, R. J., Lione, L. A., Mangiarini, L., Mahal, A., Bates, G. P., *et al*. (2000) Abnormal synaptic plasticity and impaired spatial cognition in mice transgenic for exon 1 of the human Huntington's disease mutation. *J. Neurosci.* **20**, 5115–5123
160. Song, C., Zhang, Y., Parsons, C. G., and Liu, Y. F. (2003) Expression of polyglutamine-expanded huntingtin induces tyrosine phosphorylation of N-methyl-D-aspartate receptors. *J. Biol. Chem.* **278**, 33364–33369
161. Ralser, M., Nonhoff, U., Albrecht, M., Lengauer, T., Wanker, E. E., Lehrach, H., and Krobitsch, S. (2005) Ataxin-2 and huntingtin interact with endophilin-A complexes to function in plastin-associated pathways. *Hum. Mol. Genet.* **14**, 2893–2909
162. Landles, C., Sathasivam, K., Weiss, A., Woodman, B., Moffitt, H., Finkbeiner, S., *et al*. (2010) Proteolysis of mutant huntingtin produces an

exon 1 fragment that accumulates as an aggregated protein in neuronal nuclei in Huntington disease. *J. Biol. Chem.* **285**, 8808–8823
163. Sathasivam, K., Neueder, A., Gipson, T. A., Landles, C., Benjamin, A. C., Bondulich, M. K., *et al*. (2013) Aberrant splicing of HTT generates the pathogenic exon 1 protein in Huntington disease. *Proc. Natl. Acad. Sci. U. S. A.* **110**, 2366–2370
164. Baksi, S., Basu, S., and Mukhopadhyay, D. (2014) Mutant huntingtin replaces Gab1 and interacts with C-terminal SH3 domain of growth factor receptor binding protein 2 (Grb2). *Neurosci. Res.* **87**, 77–83
165. Shen, W. C., Li, H. Y., Chen, G. C., Chern, Y., and Tu, P. H. (2015) Mutations in the ubiquitin-binding domain of OPTN/optineurin interfere with autophagy-mediated degradation of misfolded proteins by a dominant-negative mechanism. *Autophagy* **11**, 685–700
166. Neueder, A., Landles, C., Ghosh, R., Howland, D., Myers, R. H., Faull, R. L. M., *et al*. (2017) The pathogenic exon 1 HTT protein is produced by incomplete splicing in Huntington's disease patients. *Sci. Rep.* **7**, 1307
167. Franich, N. R., Hickey, M. A., Zhu, C., Osborne, G. F., Ali, N., Chu, T., *et al*. (2019) Phenotype onset in Huntington's disease knock-in mice is correlated with the incomplete splicing of the mutant huntingtin gene. *J. Neurosci. Res.* **97**, 1590–1605
168. Ceccon, A., Tugarinov, V., and Clore, G. M. (2021) Quantitative exchange NMR-based analysis of huntingtin-SH3 interactions suggests an allosteric mechanism of inhibition of huntingtin aggregation. *J. Am. Chem. Soc.* **143**, 9672–9681
169. Fao, L., Coelho, P., Duarte, L., Vilaça, R., Hayden, M. R., Mota, S. I., and Rego, A. C. (2023) Restoration of c-src/fyn proteins rescues mitochondrial dysfunction in huntington's disease. *Antioxid. Redox Signal.* **38**, 95–114
170. Fao, L., Coelho, P., Rodrigues, R. J., and Rego, A. C. (2022) Restored Fyn levels in huntington's disease contributes to enhanced synaptic GluN2B-composed NMDA receptors and CREB activity. *Cells* **11**, 3063
171. Hoschek, F., Natan, J., Wagner, M., Sathasivam, K., Abdelmoez, A., von Einem, B., *et al*. (2024) Huntingtin HTT1a is generated in a CAG repeat-length-dependent manner in human tissues. *Mol. Med.* **30**, 36
172. Sogorb-Gonzalez, M., Landles, C., Caron, N. S., Stam, A., Osborne, G., Hayden, M. R., *et al*. (2024) Exon 1-targeting miRNA reduces the pathogenic exon 1 HTT protein in Huntington disease models. *Brain* **147**, 4043–4055
173. Chitre, M., and Emery, P. (2023) ATXN2 is a target of N-terminal proteolysis. *PLoS One* **18**, e0296085
174. Scoles, D. R., Pflieger, L. T., Thai, K. K., Hansen, S. T., Dansithong, W., and Pulst, S. M. (2012) ETS1 regulates the expression of ATXN2. *Hum. Mol. Genet.* **21**, 5048–5065
175. Monteiro, P., and Feng, G. (2017) SHANK proteins: roles at the synapse and in autism spectrum disorder. *Nat. Rev. Neurosci.* **18**, 147–157
176. Guergueltcheva, V., Azmanov, D. N., Angelicheva, D., Smith, K. R., Chamova, T., Florez, L., *et al*. (2012) Autosomal-recessive congenital cerebellar ataxia is caused by mutations in metabotropic glutamate receptor 1. *Am. J. Hum. Genet.* **91**, 553–564
177. Watson, L. M., Bamber, E., Schnekenberg, R. P., Williams, J., Bettencourt, C., Lickiss, J., *et al*. (2017) Dominant mutations in GRM1 cause spinocerebellar ataxia type 44. *Am. J. Hum. Genet.* **101**, 451–458
178. Collins, M. A., An, J., Hood, B. L., Conrads, T. P., and Bowser, R. P. (2015) Label-free LC-MS/MS proteomic analysis of cerebrospinal fluid identifies protein/pathway alterations and candidate biomarkers for amyotrophic lateral sclerosis. *J. Proteome Res.* **14**, 4486–4501
179. Mongredien, R., Erdozain, A. M., Dumas, S., Cutando, L., Del Moral, A. N., Puighermanal, E., *et al*. (2019) Cartography of hevin-expressing cells in the adult brain reveals prominent expression in astrocytes and parvalbumin neurons. *Brain Struct. Funct.* **224**, 1219–1244
180. Yadav, A., Matson, K. J. E., Li, L., Hua, I., Petrescu, J., Kang, K., *et al*. (2023) A cellular taxonomy of the adult human spinal cord. *Neuron* **111**, 328–344.e7
181. Kramer-Albers, E. M., and White, R. (2011) From axon-glial signalling to myelination: the integrating role of oligodendroglial Fyn kinase. *Cell Mol. Life Sci.* **68**, 2003–2012
182. Kliche, S., Breitling, D., Togni, M., Pusch, R., Heuer, K., Wang, X., *et al*. (2006) The ADAP/SKAP55 signaling module regulates T-cell receptor-mediated integrin activation through plasma membrane targeting of Rap1. *Mol. Cell Biol.* **26**, 7130–7144
183. Ganesan, A., Muralidharan, P., and Ramya, L. N. (2023) The fulcrum of demyelination in multiple sclerosis. *Curr. Protein Pept. Sci.* **24**, 579–588
184. Wilkinson, B., and Coba, M. P. (2020) Molecular architecture of postsynaptic Interactomes. *Cell Signal.* **76**, 109782
185. Piccini, A., and Malinow, R. (2002) Critical postsynaptic density 95/disc large/zonula occludens-1 interactions by glutamate receptor 1 (GluR1) and GluR2 required at different subcellular sites. *J. Neurosci.* **22**, 5387–5392
186. Lua, B. L., and Low, B. C. (2005) Cortactin phosphorylation as a switch for actin cytoskeletal network and cell dynamics control. *FEBS Lett.* **579**, 577–585
187. Clements, C. M., Henen, M. A., Vögeli, B., and Shellman, Y. G. (2023) The structural dynamics, complexity of interactions, and functions in cancer of multi-SAM containing proteins. *Cancers (Basel)* **15**, 3019
188. Liu, X., Huai, J., Endle, H., Schlüter, L., Fan, W., Li, Y., *et al*. (2016) PRG-1 regulates synaptic plasticity via intracellular PP2A/beta1-Integrin signaling. *Dev. Cell* **38**, 275–290
189. Lin, W. H., Nebhan, C. A., Anderson, B. R., and Webb, D. J. (2010) Vasodilator-stimulated phosphoprotein (VASP) induces actin assembly in dendritic spines to promote their development and potentiate synaptic strength. *J. Biol. Chem.* **285**, 36010–36020
190. Schiapparelli, L. M., Xie, Y., Sharma, P., McClatchy, D. B., Ma, Y., Yates, J. R., 3rd, *et al*. (2022) Activity-induced cortical glutamatergic neuron nascent proteins. *J. Neurosci.* **42**, 7900–7920
191. Nobuhisa, I., Takeya, R., Ogura, K., Ueno, N., Kohda, D., Inagaki, F., and Sumimoto, H. (2006) Activation of the superoxide-producing phagocyte NADPH oxidase requires co-operation between the tandem SH3 domains of p47phox in recognition of a polyproline type II helix and an adjacent alpha-helix of p22phox. *Biochem. J.* **396**, 183–192
192. Hayashi, T., Okabe, T., Nasu-Nishimura, Y., Sakaue, F., Ohwada, S., Matsuura, K., *et al*. (2007) PX-RICS, a novel splicing variant of RICS, is a main isoform expressed during neural development. *Genes Cells* **12**, 929–939
193. Liu, X., Rothe, K., Yen, R., Fruhstorfer, C., Maetzig, T., Chen, M., *et al*. (2017) A novel AHI-1-BCR-ABL-DNM2 complex regulates leukemic properties of primitive CML cells through enhanced cellular endocytosis and ROS-mediated autophagy. *Leukemia* **31**, 2376–2387
194. Gallolu Kankanamalage, S., Lee, A. Y., Wichaidit, C., Lorente-Rodriguez, A., Shah, A. M., Stippec, S., *et al*. (2017) WNK1 is an unexpected autophagy inhibitor. *Autophagy* **13**, 969–970
195. van Vliet, A. R., Chiduza, G. N., Maslen, S. L., Pye, V. E., Joshi, D., De Tito, S., *et al*. (2022) ATG9A and ATG2A form a heteromeric complex essential for autophagosome formation. *Mol. Cell* **82**, 4324–4339.e8
196. Nozawa, T., Toh, H., Iibushi, J., Kogai, K., Minowa-Nozawa, A., Satoh, J., *et al*. (2023) Rab41-mediated ESCRT machinery repairs membrane rupture by a bacterial toxin in xenophagy. *Nat. Commun.* **14**, 6230
197. Imamura, K., Izumi, Y., Watanabe, A., Tsukita, K., Woltjen, K., Yamamoto, T., *et al*. (2017) The Src/c-Abl pathway is a potential therapeutic target in amyotrophic lateral sclerosis. *Sci. Transl. Med.* **9**, eaaf3962
198. Wang, K. Z., Wara-Aswapati, N., Boch, J. A., Yoshida, Y., Hu, C. D., Galson, D. L., and Auron, P. E. (2006) TRAF6 activation of PI 3-kinase-dependent cytoskeletal changes is cooperative with Ras and is mediated by an interaction with cytoplasmic Src. *J. Cell Sci.* **119**(Pt 8), 1579–1591
199. Chen, R., Wang, H., Liang, B., Liu, G., Tang, M., Jia, R., *et al*. (2016) Downregulation of ASPP2 improves hepatocellular carcinoma cells survival via promoting BECN1-dependent autophagy initiation. *Cell Death Dis.* **7**, e2512
200. Pang, Y., Pan, L., Zhang, Y., and Liu, G. (2019) TP53BP2 decreases cell proliferation and induces autophagy in neuroblastoma cell lines. *Oncol. Lett.* **17**, 4976–4984
201. Kim, J. Y., Welsh, E. A., Oguz, U., Fang, B., Bai, Y., Kinose, F., *et al*. (2013) Dissection of TBK1 signaling via phosphoproteomics in lung cancer cells. *Proc. Natl. Acad. Sci. U. S. A.* **110**, 12414–12419
202. Freischmidt, A., Wieland, T., Richter, B., Ruf, W., Schaeffer, V., Müller, K., *et al*. (2015) Haploinsufficiency of TBK1 causes familial ALS and frontotemporal dementia. *Nat. Neurosci.* **18**, 631–636
203. Heath, R. J., Goel, G., Baxt, L. A., Rush, J. S., Mohanan, V., Paulus, G. L. C., *et al*. (2016) RNF166 determines recruitment of adaptor proteins during antibacterial autophagy. *Cell Rep.* **17**, 2183–2194

204. Ma, S., Attarwala, I. Y., and Xie, X. Q. (2019) SQSTM1/p62: a potential target for neurodegenerative disease. *ACS Chem. Neurosci.* **10**, 2094–2114
205. Nakazawa, S., Oikawa, D., Ishii, R., Ayaki, T., Takahashi, H., Takeda, H., *et al*. (2016) Linear ubiquitination is involved in the pathogenesis of optineurin-associated amyotrophic lateral sclerosis. *Nat. Commun.* **7**, 12547
206. Richter, B., Sliter, D. A., Herhaus, L., Stolz, A., Wang, C., Beli, P., *et al*. (2016) Phosphorylation of OPTN by TBK1 enhances its binding to Ub chains and promotes selective autophagy of damaged mitochondria. *Proc. Natl. Acad. Sci. U. S. A.* **113**, 4039–4044
207. Moore, A. S., and Holzbaur, E. L. (2016) Dynamic recruitment and activation of ALS-associated TBK1 with its target optineurin are required for efficient mitophagy. *Proc. Natl. Acad. Sci. U. S. A.* **113**, E3349–E3358
208. Weil, R., Laplantine, E., Curic, S., and Génin, P. (2018) Role of optineurin in the mitochondrial dysfunction: potential implications in neurodegenerative diseases and cancer. *Front. Immunol.* **9**, 1243
209. White, J., Suklabaidya, S., Vo, M. T., Choi, Y. B., and Harhaj, E. W. (2023) Multifaceted roles of TAX1BP1 in autophagy. *Autophagy* **19**, 44–53
210. Gao, L., Coope, H., Grant, S., Ma, A., Ley, S. C., and Harhaj, E. W. (2011) ABIN1 protein cooperates with TAX1BP1 and A20 proteins to inhibit antiviral signaling. *J. Biol. Chem.* **286**, 36592–36602
211. Benyamin, B., He, J., Zhao, Q., Gratten, J., Garton, F., Leo, P. J., *et al*. (2017) Cross-ethnic meta-analysis identifies association of the GPX3-TNIP1 locus with amyotrophic lateral sclerosis. *Nat. Commun.* **8**, 611
212. Restuadi, R., Steyn, F. J., Kabashi, E., Ngo, S. T., Cheng, F. F., Nabais, M. F., *et al*. (2022) Functional characterisation of the amyotrophic lateral sclerosis risk locus GPX3/TNIP1. *Genome Med.* **14**, 7
213. Zhou, J., Rasmussen, N. L., Olsvik, H. L., Akimov, V., Hu, Z., Evjen, G., *et al*. (2023) TBK1 phosphorylation activates LIR-dependent degradation of the inflammation repressor TNIP1. *J. Cell Biol.* **222**, e202108144
214. Rasmussen, N. L., Zhou, J., Olsvik, H., Kaeser-Pebernard, S., Lamark, T., Dengjel, J., and Johansen, T. (2023) The inflammation repressor TNIP1/ABIN-1 is degraded by autophagy following TBK1 phosphorylation of its LIR. *Autophagy* **19**, 2819–2820
215. Le Guerroue, F., Bunker, E. N., Rosencrans, W. M., Nguyen, J. T., Basar, M. A., Werner, A., *et al*. (2023) TNIP1 inhibits selective autophagy via bipartite interaction with LC3/GABARAP and TAX1BP1. *Mol. Cell* **83**, 927–941.e8
216. Wu, S., Li, M., Wang, L., Yang, L., Cui, J., Li, F., *et al*. (2024) Structural basis for TNIP1 binding to FIP200 during mitophagy. *J. Biol. Chem.* **300**, 107605
217. White, J., Choi, Y. B., Zhang, J., Vo, M. T., He, C., Shaikh, K., and Harhaj, E. W. (2025) Phosphorylation of the selective autophagy receptor TAX1BP1 by TBK1 and IKBKE/IKKi promotes ATG8-family protein-dependent clearance of MAVS aggregates. *Autophagy* **21**, 160–177
218. Svenning, S., Lamark, T., Krause, K., and Johansen, T. (2011) Plant NBR1 is a selective autophagy substrate and a functional hybrid of the mammalian autophagic adapters NBR1 and p62/SQSTM1. *Autophagy* **7**, 993–1010
219. Rasmussen, N. L., Kournoutis, A., Lamark, T., and Johansen, T. (2022) NBR1: the archetypal selective autophagy receptor. *J. Cell Biol.* **221**, e202208092
220. Cozzi, M., and Ferrari, V. (2022) Autophagy dysfunction in ALS: from transport to protein degradation. *J. Mol. Neurosci.* **72**, 1456–1481
221. Yang, S., Fifita, J. A., Williams, K. L., Warraich, S. T., Pamphlett, R., Nicholson, G. A., and Blair, I. P. (2013) Mutation analysis and immunopathological studies of PFN1 in familial and sporadic amyotrophic lateral sclerosis. *Neurobiol. Aging* **34**, 2235.e7
222. Farg, M. A., Sundaramoorthy, V., Sultana, J. M., Yang, S., Atkinson, R. A. K., Levina, V., *et al*. (2014) C9ORF72, implicated in amytrophic lateral sclerosis and frontotemporal dementia, regulates endosomal trafficking. *Hum. Mol. Genet.* **23**, 3579–3595
223. Renaud, L., Picher-Martel, V., Codron, P., and Julien, J. P. (2019) Key role of UBQLN2 in pathogenesis of amyotrophic lateral sclerosis and frontotemporal dementia. *Acta Neuropathol. Commun.* **7**, 103
224. Alexander, E. J., Ghanbari Niaki, A., Zhang, T., Sarkar, J., Liu, Y., Nirujogi, R. S., *et al*. (2018) Ubiquilin 2 modulates ALS/FTD-linked FUS-RNA complex dynamics and stress granule formation. *Proc. Natl. Acad. Sci. U. S. A.* **115**, E11485–E11494
225. Zheng, T., Galagedera, S. K. K., and Castaneda, C. A. (2021) Previously uncharacterized interactions between the folded and intrinsically disordered domains impart asymmetric effects on UBQLN2 phase separation. *Protein Sci.* **30**, 1467–1481
226. Osaka, M., Ito, D., Yagi, T., Nihei, Y., and Suzuki, N. (2015) Evidence of a link between ubiquilin 2 and optineurin in amyotrophic lateral sclerosis. *Hum. Mol. Genet.* **24**, 1617–1629
227. Kim, J. E., Ko, A. R., Hyun, H. W., Min, S. J., and Kang, T. C. (2018) P2RX7-MAPK1/2-SP1 axis inhibits MTOR independent HSPB1-mediated astroglial autophagy. *Cell Death Dis.* **9**, 546
228. Alberti, S., Mateju, D., Mediani, L., and Carra, S. (2017) Granulostasis: protein quality control of RNP granules. *Front. Mol. Neurosci.* **10**, 84
229. Muranova, L. K., Shatov, V. M., and Gusev, N. B. (2022) Role of small heat shock proteins in the remodeling of actin microfilaments. *Biochemistry (Mosc)* **87**, 800–811
230. Fox, L. M., Kim, K., Johnson, C. W., Chen, S., Croce, K. R., Victor, M. B., *et al*. (2020) Huntington's disease pathogenesis is modified in vivo by Alfy/Wdfy3 and selective macroautophagy. *Neuron* **105**, 813–821.e6
231. Clausen, T. H., Lamark, T., Isakson, P., Finley, K., Larsen, K. B., Brech, A., *et al*. (2010) p62/SQSTM1 and ALFY interact to facilitate the formation of p62 bodies/ALIS and their degradation by autophagy. *Autophagy* **6**, 330–344
232. Filimonenko, M., Isakson, P., Finley, K. D., Anderson, M., Jeong, H., Melia, T. J., *et al*. (2010) The selective macroautophagic degradation of aggregated proteins requires the PI3P-binding protein Alfy. *Mol. Cell* **38**, 265–279
233. Popelka, H., and Klionsky, D. J. (2025) The emerging significance of Vac8, a multi-purpose armadillo-repeat protein in yeast. *Autophagy* **21**, 913–916
234. Park, J., Chen, Y., Tishkoff, D. X., Peng, C., Tan, M., Dai, L., *et al*. (2013) SIRT5-mediated lysine desuccinylation impacts diverse metabolic pathways. *Mol. Cell* **50**, 919–930
235. Kim, K. R., Cho, E. J., Eom, J. W., Oh, S. S., Nakamura, T., Oh, C. K., *et al*. (2022) S-Nitrosylation of cathepsin B affects autophagic flux and accumulation of protein aggregates in neurodegenerative disorders. *Cell Death Differ* **29**, 2137–2150
236. Katunuma, N. (2010) Posttranslational processing and modification of cathepsins and cystatins. *J. Signal. Transduct.* **2010**, 375345
237. Xie, Z., Zhao, M., Yan, C., Kong, W., Lan, F., Narengaowa, *et al*. (2023) Cathepsin B in programmed cell death machinery: mechanisms of execution and regulatory pathways. *Cell Death Dis.* **14**, 255
238. Sen, N. E., Drost, J., Gispert, S., Torres-Odio, S., Damrath, E., Klinkenberg, M., *et al*. (2016) Search for SCA2 blood RNA biomarkers highlights Ataxin-2 as strong modifier of the mitochondrial factor PINK1 levels. *Neurobiol. Dis.* **96**, 115–126
239. Singh, A., Hulsmeier, J., Kandi, A. R., Pothapragada, S. S., Hillebrand, J., Petrauskas, A., *et al*. (2021) Antagonistic roles for Ataxin-2 structured and disordered domains in RNP condensation. *Elife* **10**, e60326
240. Shibata, H., Huynh, D. P., and Pulst, S. M. (2000) A novel protein with RNA-binding motifs interacts with ataxin-2. *Hum. Mol. Genet.* **9**, 1303–1313
241. Ponnambalam, S., and Baldwin, S. A. (2003) Constitutive protein secretion from the trans-Golgi network to the plasma membrane. *Mol. Membr. Biol.* **20**, 129–139
242. Yin, D. M., Huang, Y. H., Zhu, Y. B., and Wang, Y. (2008) Both the establishment and maintenance of neuronal polarity require the activity of protein kinase D in the Golgi apparatus. *J. Neurosci.* **28**, 8832–8843
243. Bisbal, M., Conde, C., Donoso, M., Bollati, F., Sesma, J., Quiroga, S., *et al*. (2008) Protein kinase d regulates trafficking of dendritic membrane proteins in developing neurons. *J. Neurosci.* **28**, 9297–9308
244. Czondor, K., Ellwanger, K., Fuchs, Y. F., Lutz, S., Gulyás, M., Mansuy, I. M., *et al*. (2009) Protein kinase D controls the integrity of Golgi apparatus and the maintenance of dendritic arborization in hippocampal neurons. *Mol. Biol. Cell* **20**, 2108–2120
245. Fujishima, K., Horie, R., Mochizuki, A., and Kengaku, M. (2012) Principles of branch dynamics governing shape characteristics of cerebellar Purkinje cell dendrites. *Development* **139**, 3442–3455
246. Bencsik, N., Szíber, Z., Liliom, H., Tárnok, K., Borbély, S., Gulyás, M., *et al*. (2015) Protein kinase D promotes plasticity-induced F-actin stabilization in dendritic spines and regulates memory formation. *J. Cell Biol.* **210**, 771–783

247. Oueslati Morales, C. O., Ignácz, A., Bencsik, N., Sziber, Z., Rátkai, A. E., Lieb, W. S., *et al*. (2021) Protein kinase D promotes activity-dependent AMPA receptor endocytosis in hippocampal neurons. *Traffic* **22**, 454–470
248. Besirli, C. G., and Johnson, E. M., Jr. (2006) The activation loop phosphorylation of protein kinase D is an early marker of neuronal DNA damage. *J. Neurochem.* **99**, 218–225
249. Krueger, D. D., Osterweil, E. K., and Bear, M. F. (2010) Activation of mGluR5 induces rapid and long-lasting protein kinase D phosphorylation in hippocampal neurons. *J. Mol. Neurosci.* **42**, 1–8
250. Liliom, H., Tárnok, K., Ábrahám, Z., Rácz, B., Hausser, A., and Schlett, K. (2017) Protein kinase D exerts neuroprotective functions during oxidative stress via nuclear factor kappa B-independent signaling pathways. *J. Neurochem.* **142**, 948–961
251. Pose-Utrilla, J., García-Guerra, L., Del Puerto, A., Martín, A., Jurado-Arjona, J., De León-Reyes, N. S., *et al*. (2017) Excitotoxic inactivation of constitutive oxidative stress detoxification pathway in neurons can be rescued by PKD1. *Nat. Commun.* **8**, 2275
252. Johnson, J. R., and Barclay, J. W. (2023) C. elegans dkf-1 (Protein Kinase D1) mutants have age-dependent defects in locomotion and neuromuscular transmission. *Micro Publ. Biol.* **2023**. https://doi.org/10.17912/micropub.biology.000800
253. Uesugi, A., Kataoka, A., Tozaki-Saitoh, H., Koga, Y., Tsuda, M., Robaye, B., *et al*. (2012) Involvement of protein kinase D in uridine diphosphate-induced microglial macropinocytosis and phagocytosis. *Glia* **60**, 1094–1105
254. Yang, Y., Halliday, G. M., Kiernan, M. C., and Tan, R. H. (2019) TDP-43 levels in the brain tissue of ALS cases with and without C9ORF72 or ATXN2 gene expansions. *Neurology* **93**, e1748–e1755
255. Lauranzano, E., Pozzi, S., Pasetto, L., Stucchi, R., Massignan, T., Paolella, K., *et al*. (2015) Peptidylprolyl isomerase A governs TARDBP function and assembly in heterogeneous nuclear ribonucleoprotein complexes. *Brain* **138**(Pt 4), 974–991
256. Goedert, M. (1993) Tau protein and the neurofibrillary pathology of Alzheimer's disease. *Trends Neurosci.* **16**, 460–465
257. Lee, G. (2005) Tau and src family tyrosine kinases. *Biochim. Biophys. Acta* **1739**, 323–330
258. Sieben, A., Van Langenhove, T., Engelborghs, S., Martin, J. J., Boon, P., Cras, P., *et al*. (2012) The genetics and neuropathology of frontotemporal lobar degeneration. *Acta Neuropathol.* **124**, 353–372
259. Neumann, M., Sampathu, D. M., Kwong, L. K., Truax, A. C., Micsenyi, M. C., Chou, T. T., *et al*. (2006) Ubiquitinated TDP-43 in frontotemporal lobar degeneration and amyotrophic lateral sclerosis. *Science* **314**, 130–133
260. Li, H. Y., Yeh, P. A., Chiu, H. C., Tang, C. Y., and Tu, B. P. H. (2011) Hyperphosphorylation as a defense mechanism to reduce TDP-43 aggregation. *PLoS One* **6**, e23075
261. Wang, A., Conicella, A. E., Schmidt, H. B., Martin, E. W., Rhoads, S. N., Reeb, A. N., *et al*. (2018) A single N-terminal phosphomimic disrupts TDP-43 polymerization, phase separation, and RNA splicing. *EMBO J.* **37**, e97452
262. Gruijs da Silva, L. A., Simonetti, F., Hutten, S., Riemenschneider, H., Sternburg, E. L., Pietrek, L. M., *et al*. (2022) Disease-linked TDP-43 hyperphosphorylation suppresses TDP-43 condensation and aggregation. *EMBO J.* **41**, e108443
263. Haider, R., Penumutchu, S., Boyko, S., and Surewicz, W. K. (2024) Phosphomimetic substitutions in TDP-43's transiently alpha-helical region suppress phase separation. *Biophys. J.* **123**, 361–373
264. Kim, K. Y., Lee, H. W., Shim, Y. M., Mook-Jung, I., Jeon, G. S., and Sung, J. J. (2015) A phosphomimetic mutant TDP-43 (S409/410E) induces Drosha instability and cytotoxicity in Neuro 2A cells. *Biochem. Biophys. Res. Commun.* **464**, 236–243
265. Paron, F., Barattucci, S., Cappelli, S., Romano, M., Berlingieri, C., Stuani, C., *et al*. (2022) Unraveling the toxic effects mediated by the neurodegenerative disease-associated S375G mutation of TDP-43 and its S375E phosphomimetic variant. *J. Biol. Chem.* **298**, 102252
266. Hofweber, M., and Dormann, D. (2019) Friend or foe-Post-translational modifications as regulators of phase separation and RNP granule dynamics. *J. Biol. Chem.* **294**, 7137–7150
267. Ainani, H., Bouchmaa, N., Ben Mrid, R., and El Fatimy, R. (2023) Liquid-liquid phase separation of protein tau: an emerging process in Alzheimer's disease pathogenesis. *Neurobiol. Dis.* **178**, 106011